Building and Environment 207 (2022) 108427

Contents lists available at ScienceDirect

Building and Environment

journal homepage: www.elsevier.com/locate/buildenv

Evaluating the thermal-radiative performance of ENVI-met model for green infrastructure typologies: Experience from a subtropical climate

Wanlu Ouyang [a,*], Tim Sinsel [b], Helge Simon [b], Tobi Eniolu Morakinyo [c], Huimin Liu [d], Edward Ng [a,e,f]

[a] School of Architecture, The Chinese University of Hong Kong, New Territories, Hong Kong, China
[b] Department of Geography, Johannes Gutenberg University Mainz, 55099, Mainz, Germany
[c] School of Geography, University College Dublin, Dublin 4, Ireland
[d] Institute of Space and Earth Information Science, The Chinese University of Hong Kong, New Territories, Hong Kong, China
[e] Institute of Future Cities, The Chinese University of Hong Kong, New Territories, Hong Kong, China
[f] Institute of Environment, Energy and Sustainability, The Chinese University of Hong Kong, New Territories, Hong Kong, China

ARTICLE INFO

Keywords:
ENVI-met
Model evaluation
Sensitivity analysis
Thermal-radiative performance
Urban greening
Urban climate

ABSTRACT

Microclimate knowledge has been intensively integrated into urban planning and design to improve the buildings' energy performance and outdoor thermal comfort. To assess the climatic mitigation strategies, numerical modeling is gaining higher relevance. ENVI-met, a microclimate model to simulate the complex surface-vegetation-atmosphere interactions in the built environment, is receiving increasing popularity.

This study aims to systematically evaluate the thermal-radiative performance of the ENVI-met model based on its recent updates. First, a field measurement was conducted in a subtropical city. Thermal-radiative parameters were collected besides three green infrastructure (GI) typologies (i.e., green roof, green wall, ground tree) and three corresponding reference sites. Second, sensitivity tests were conducted for the inputs and settings of ENVI-met model, including new radiation module IVS (Indexed View Sphere), meteorological boundary conditions, materials settings, and output intervals. Third, the thermal-radiative performance of ENVI-met was compared among the six measurement sites, three output intervals, and nine microclimate variables, based on four evaluation metrics.

The results showed that 1) recent updates of ENVI-met can improve the estimation accuracy, especially with IVS on, radiation forcing, and localized materials settings; 2) ENVI-met was capable of simulating the thermal-radiative performance of three GI typologies simultaneously; 3) mobile measurement can be used for ENVI-met validation, and 4) model evaluation results were sensitive to the metrics.

Overall, this study emphasized proper validation for ENVI-met before applications, when full forcing and localized settings are essential. The strengths and limitations of ENVI-met were discussed and implications were provided for model developers and users.

1. Introduction

1.1. Background

Due to rapid urbanization processes, global climate change, and intensified heat waves, climate knowledge has been gaining increasing attentions in both academic fields [1] and urban planning and design practices [2]. In this respect, numerical simulation tools are powerful means for researchers and urban planners to understand the urban climate mechanisms and assess the climate adaptation strategies. Thus, numerical simulation has gained increasingly popularity over the past two decades [3]. This popularity is justified by the high capacity of modeling to involve the nonlinearity and complexity of urban climate processes [4], and is also supported by the development in both hardware (i.e., increasing computational power of computers) and software (i.e., emerging models or tools) [5]. Moreover, numerical modeling can assist the climate-sensitive urban planning, as it can assess the effectiveness of mitigation strategies based on "what-if" scenarios, especially

* Corresponding author.
E-mail addresses: wanlu.oy@link.cuhk.edu.hk (W. Ouyang), t.sinsel@geo.uni-mainz.de (T. Sinsel), h.simon@geo.uni-mainz.de (H. Simon), tobi.morakinyo@ucd.ie (T.E. Morakinyo), hmliu@cuhk.edu.hk (H. Liu), edwardng@cuhk.edu.hk (E. Ng).

https://doi.org/10.1016/j.buildenv.2021.108427
Received 16 August 2021; Received in revised form 23 September 2021; Accepted 5 October 2021
Available online 9 October 2021

during the planning stages.

In urban climate fields, numerical simulation tools can be classified into two types according to their mechanisms: energy balance model (EBM) based on the energy balance budget, and computational fluid dynamics (CFD) based on the equations of fluid dynamics and conservation of mass, momentum, energy. EBM is mainly for large-scale studies (i.e., city scale), as it approximates the complex buildings with limited grids and applies homogeneous geometry for the whole city [5]. Due to absences of air velocity, EBM cannot reproduce the interactions between air velocity and temperature fields, and hence is not suitable for microclimate studies [5]. On the contrary, CFD provides detailed and accurate information in the relevant thermal, velocity, radiation fields, and thus is a powerful tool at microclimate scales for buildings' energy consumption and outdoor thermal comfort [4]. Among all of the CFD based models, ENVI-met is one of the most widely used tools in multiple climate backgrounds and for different urban forms with diversified characteristics in buildings and greenery [6].

1.2. ENVI-met model and applications

ENVI-met is designed to simulate the complex atmosphere-vegetation-surface interactions. Specifically, it is a grid-based model with fine resolution (0.5–10 m) and uses standard κ-ε turbulence model and Reynolds Averaged Navier-Stokes (RANS) equations [7]. There are several sub-models in ENVI-met: 1) 1D (one-dimensional) boundary model to initialize the simulation and establish the boundary conditions of the 3D model; 2) 3D atmospheric model to simulate all the processes of temperature, humidity, turbulence, radiation fluxes, and pollutants; 3) soil model to calculate the temperature and humidity fluxes in the soil layers; 4) vegetation model to simulate the transpiration rates, leaf temperature of the plants, as well as the heat and vapor interactions between vegetation and atmosphere [6,7]. Compared with previous versions, the recent version of ENVI-met (V4) has been updated greatly [8]. Firstly, a 3D vegetation module has been added for mimicking complex vegetation geometries. Secondly, a "full forcing" scheme has been added to allow the half-hourly measured values as the inputs, i.e., air temperature, relative humidity, cloud cover/solar radiations, and wind conditions. Thirdly, multiple façade layers have been added to the building module, up to three different materials can be applied with different physical parameters, including reflectivity, absorption, and specific heat capacity. Lastly, ENVI-met version 4.4 has implemented a roof and façade greening module. Hence, these updates of ENVI-met are expected to generate more reliable simulation results [9].

ENVI-met has been widely applied to investigate the impacts of urban greening on urban microclimate [6]. Specifically, three green infrastructure (GI) typologies, i.e., ground trees, green walls, and green roofs, are often investigated individually and collectively. For instance, regarding ground trees, ENVI-met was used to investigate the impacts of coverage ratio amount [10,11], tree species [12–14], and planting location [15,16] on the magnitude of the thermal benefits. In terms of vertical greenery, the model was applied to explore the impacts of green façade ratio [17], implementation orientation [17,18], and planting height [18] on cooling effect. For green roof, ENVI-met can examine the effects of roof coverage ratio [19–21], green roof types and plant characteristics [19,22], and planting arrangement [20,21] on cooling provision. Overall, the thermal performance was mainly quantified by air temperature, relative humidity, surface temperature, etc., while the radiative performance commonly considered mean radiant temperature, longwave and shortwave radiations, etc. All these parameters are essential for both buildings' energy consumption and outdoor thermal comfort.

1.3. Model evaluation and ENVI-met performance

Performance evaluation is an essential step to ensure the reliability of a model, and minimize the probability of making wrong decisions based on the simulation results or gaining an adverse insight in the targeted situations [23]. Model performance can be distinguished into scientific and operational aspects. The scientific performance is related with the model components, while the operational performance links to the particular applications [24]. In our study, the operational performance was evaluated, which refers to comparing the simulation results with the observed data in a given application context [24].

Previous studies have examined the performance of ENVI-met in different perspectives [6]. For instance, the model was evaluated for different seasons [25,26], different meteorological conditions [27], urban spaces [28], ground surfaces [29], tree typologies [30], tree species [31], and applicability in diverse urban forms [26], near a tree [4], near façade greening [32], or for specific microclimate variables (i.e., mean radiant temperature) [26,33]. Based on their evaluation results, as summarized in Appendix Table A1, ENVI-met provides relatively accurate estimations of air temperature (AT) and mean radiant temperature (MRT), especially during diurnal periods in summertime. For instance, for AT, two common evaluation metrics performed reasonably, with R^2 ranging from 0.73–0.99 and root mean squared error (RMSE) ranging from 0.69–3.97 K; for MRT, R^2 ranged from 0.54–0.95, and RMSE ranged from 6.44–16.10 K. Although the evidence came from different climate backgrounds and various built environment, they proved the reliability of ENVI for microclimate analysis and applications.

However, current literatures have evaluated the performance of ENVI-met mainly about the estimations of AT and MRT [6], yet other microclimate parameters haven been largely overlooked for the performance of ENVI-met [29]. Based on the limited evidence available, ENVI-met tends to overestimate radiation in the morning and afternoon but underestimates it during noon [31,33]. Accordingly, MRT was also over- and under-estimated [27]. To address the limitation regarding the radiation estimations, the Indexed View Sphere (IVS) scheme was introduced in the version 4.4 [33]. Moreover, in order to tackle the limitations of static solar radiation and wind characteristics [27,28], recent versions of ENVI-met introduced the full forcing scheme to improve the boundary conditions by involving more meteorological variables, such as half-hourly solar radiation or cloud amount, wind speed and directions [34].

1.4. Research objectives

Four research gaps have been mainly identified so far. First, although some studies validated ENVI-met before parametric studies [35–37], there is scarcely a systematic evaluation study for the recent updates of ENVI-met, i.e., IVS scheme for multiple interactions between surfaces, new full forcing scheme for detailed meteorological boundary conditions, new Advanced Canopy Radiation Transfer (ACRT) module for complex radiation interactions within vegetation canopies [38], and new features in façade and rooftop greening [39]. Second, three GI typologies have been examined individually in ENVI-met [20,30,32], yet it is pending to be explored how ENVI-met performs when including them simultaneously within one homogeneous site. Third, mobile measurement is one of the widely used method to collect microclimate parameters [40–42]. It is worth examining whether the data from mobile measurement can be applied for ENVI-met model validation. Fourth, several metrics have been utilized for model evaluation previously, but their sensitivities are scarcely compared.

Therefore, this study aims to systematically evaluate the recent updates of ENVI-met, and assess the thermal-radiative performance of ENVI-met model for three GI typologies within a homogeneous site in a subtropical climate city, Hong Kong. Four specific objectives were addressed: 1) to examine the influence of the inputs and settings on the reliability of ENVI-met; 2) to measure the estimation accuracy of thermal-radiative variables for three GI typologies; 3) to investigate whether the output intervals affect the evaluation results; 4) to explore the sensitivity of different metrics towards the model evaluation results.

To achieve these objectives, firstly, a field measurement was taken in six points, three near GI typologies (i.e., green roof, green wall, and ground tree) and three at corresponding reference sites. Secondly, sensitivity analyses were conducted for the model inputs and settings, including four aspects: new radiation scheme (IVS), meteorological boundary conditions, materials parameters, and output intervals. Thirdly, based on the optimal model in the sensitivity analyses, the reliability of ENVI-met was evaluated for six measurement points, nine microclimate variables, and three output intervals by four quantitative evaluation metrics. Finally, the strengths and limitations of ENVI-met were discussed for its applications in the subtropical climate context. This study helps model users including researchers, practitioners (e.g., urban planners and designers), and policy makers extend the understanding in the capabilities and limitations of ENVI-met model, thereby assist developing and implementing climate-sensitive planning strategies.

2. Methodology

2.1. Study area and measurement site

This study was conducted in Hong Kong (HK), located in the eastern Pearl River Delta by the South China Sea (22.3193° N, 114.1694° E). With a typical humid subtropical climate (Köppen *Cfa*), HK experiences a hot and humid summer with a daily temperature of 28.5 °C and a relative humidity of 80% on average [43]. To curb the menace of urban overheat, several urban greening policies have been implemented from building to city scales, e.g., Green master plan (GMP) was developed to provide an overall greening framework for specific areas [44], Practice Note APP-152 was proposed to ensure enough greening coverage ratio for new building developments [45].

The field measurement site was in the Electronic and Mechanical Services Department (EMSD) headquarters located in Kowloon peninsula (see Fig. 1). This site serves as a successful case for greening implementation in HK, as three GI typologies, namely green roof, green wall, and ground tree, are incorporated in proximity within the EMSD courtyard. Three measurement points were besides each GI typology, while three reference locations were within 5 m distance from corresponding GI point, so that the surrounding environment between paired locations was similar with minimal biases. It is noteworthy that the site provides a homogeneous urban environment with restricted vehicular and pedestrian traffic, thus the impacts of anthropogenic heat are limited for both measurements and modelling.

2.2. Field measurement and data processing

Thermal-radiative variables were collected near three GI typologies spots and three reference spots (shown in Fig. 1) between 09:30–17:25 h (LST) on four typical summer days: 07th, 09th, 11th, and 12th September in 2019. Both stationary monitoring and mobile measurements approaches were applied for data collection. To measure thermal

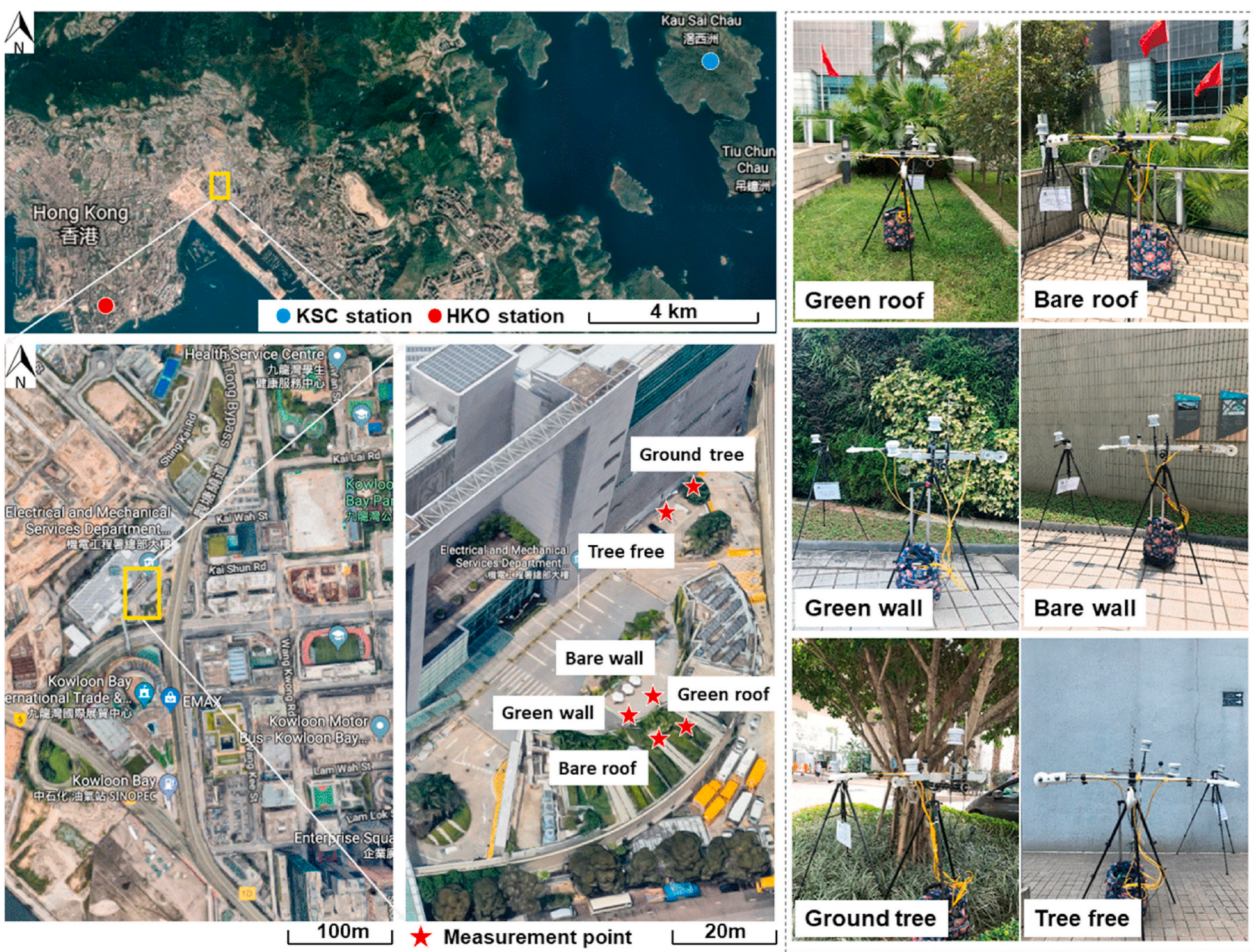

Fig. 1. Study area and measurement sites (*Adapted from* Ref. [40]).

variables, i.e., air temperature and relative humidity, a HOBO U12-012 logger was set at each of the six measurement points for the stationary monitoring. To measure radiative variables, i.e., six-directional shortwave and longwave radiation, three "four-in-one" radiometers (CNR4) were installed on a balanced tripod stand for the mobile measurement. The instruments were moved from one point to another in cycle within 1 h. Each hour cycle started at green roof and ended at tree-free point, and altogether eight cycles were realized on each measurement day. For each point, at least 2min was ensured for the equipment stabilization, afterwards 5min observations were made before shifting to the next point. The details of the mobile approach, measurement instruments, measurement process, and results were reported in our earlier study [40].

Subsequently, the collected thermal-radiative data was extracted and averaged based on three time-scales: 10min, 30min, and 1 h, which was in accordance with one of the objectives of this study - to test the sensitivity of ENVI-met towards different outputs intervals, so that the feasibility of mobile measurement for ENVI-met validation can be investigated. Mean radiant temperature was calculated based on the radiative elements in six directions with equation (1):

$$MRT = \sqrt[\frac{1}{4}]{\sum_{i=1}^{6} W_i(a_k K_i + a_l L_i) \Big/ a_l \sigma} - 273.15 \tag{1}$$

where W_i represents a weighting factor summing up to 1 (equals 0.06 for up/down direction, 0.22 for four lateral directions); K_i and L_i indicate six-directional shortwave and longwave radiation flux densities, respectively; a_k and a_l are the absorption coefficients of the clothed human body (suggested 0.7 and 0.97 respectively); σ represents the Stefan–Boltzmann constant (equals $5.67{*}10^{-8}\ W/m^2K^4$).

2.3. ENVI-met model configuration

This study evaluated the latest version of ENVI-met (V4.4.6). The actual environment of EMSD, the measurement site, was defined in the area input model. The simulation domain consisted of 250 × 225 × 46 grids with horizontal resolution (Δx and Δy) of 2 m, which is a good tradeoff between the simulation efficiency (simulation time) and the simulation accuracy [46]. The vertical grids were in varying vertical resolution (Δz) with 0.2 m resolution below 1 m height, 1 m resolution between 1 m and 10 m, and 30% telescoping above 55 m. To minimize the boundary effects and increase the numerical stability, 10 empty cells were added for each lateral boundary. The building heights ranged from 3 m to 180 m in the domain, and the building with green wall and green roof was 7 m high. The model domain was rotated 45° in the clockwise direction. The actual and modelled built environment were shown in Fig. 2.

Given that ENVI-met was developed in Germany, the default input parameters for the thermal-radiative properties of construction materials and the features of plants may not be adaptable for other cities [25]. To test the adaptability of the model's default database, sensitivity tests were conducted for both default and localized values. For localized properties, the values were adapted from both existing database, (i.e., default characteristics for building envelope published by Hong Kong Green Building Council [47]) and the values applied in previous local studies [4,27,29,48]. Considering that the material properties in the real site are complex, this study applied representative values for the typical condition in reality. We assumed the ground is built with concrete, the roof is constructed with asphalt and concrete tiles, and the building wall is constructed with heavy concrete and cement; the material properties are the average of the component materials accordingly [49]. In addition, the green roof and green wall were mimicked by 1D plant (grass) in the new green façade and roof module, while the ground tree was modelled in the 'ALBERO' module. The default and localized values of constructions and plants were listed in Table 1.

To initialize the model, either simple or full forcing scheme can be adopted for boundary meteorological conditions. The simple forcing

Table 1
Default and localized characteristics of the construction and plant.

Construction & Plant	Input Parameter [Unit]	Settings	
		Default	Localized
Ground pavement	Albedo	0.4	0.15
	Emissivity	0.9	0.9
Building roof	Thickness [m]	0.3	0.3
	Albedo	0.5	0.2
	Emissivity	0.9	0.7
	Thermal conductivity [W/(m.K)]	1.6	1.13
	Specific heat [J/(kg.K)]	850	1060
	Density [kg/m^3]	2220	2225
Building wall	Thickness [m]	0.3	0.3
	Albedo	0.5	0.2
	Emissivity	0.9	0.9
	Thermal conductivity [W/(m.K)]	1.6	1.44
	Specific heat [J/(kg.K)]	850	840
	Density [kg/m^3]	2220	2130
Green roof	Plant height [m]	0.25	0.25
	Leaf area index (LAI) [m^2/m^2]	1.5	2.5
	Plant albedo	0.2	0.2
Green wall	Plant height [m]	0.25	0.25
	Leaf area index (LAI) [m^2/m^2]	1.5	2.5
	Plant albedo	0.2	0.2
Ground tree	Plant height [m]	15	8
	Plant width [m]	11	11
	Leaf area index (LAI) [m^2/m^2]	4.2	4
	Plant albedo	0.18	0.28
	Foliage transmittance	0.3	0.1

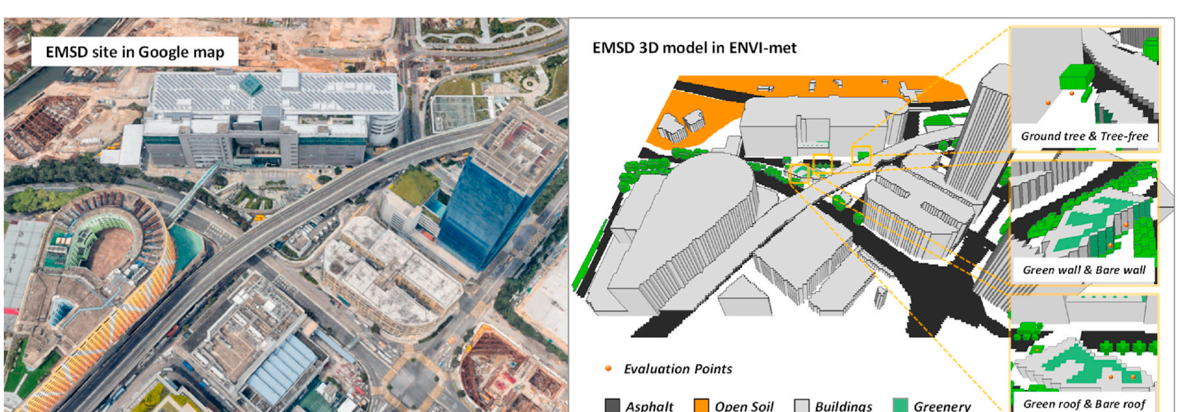

Fig. 2. The real (left) and modelled (right) built environment of measurement site.

only requires basic information, while the full forcing scheme needs half-hourly inputs, i.e., solar radiation (solar forcing) or cloud amount (cloud forcing). Current study applied and compared three forcing schemes, including simple, and two full (cloud, and solar) forcing schemes, whose inputs requirements were listed in Table 2. The meteorological data was obtained from Hong Kong Observatory (HKO) and Kau Sai Chau (KSC) weather stations (locations were shown in Fig. 1). Air temperature, relative humidity, wind speed and direction, soil temperature, cloud amount were obtained from HKO, and downward direct and diffuse shortwave radiation were acquired from KSC [50]. As cloud forcing requires the cloud cover conditions in low, medium and high levels, and HKO only provides the total cloud amount, we set all cloud cover at the medium level. When radiation forcing requires downward longwave radiation that is not measured and provided by Hong Kong Observatory authority, we used the estimation values by ENVI-met based on equation (2) [7,8]. We modified the apparent overestimations based on the measurement value on rooftops, as previous study indicated using calculated downward longwave radiation will increase prediction uncertainty [51]. The detailed forcing settings can be found in **supplementary file S1**.

$$Q_{lw}^{\downarrow} = \sum_{n=1}^{N} \sigma T^4(n)[\varepsilon_n(m+\Delta m) - \varepsilon_n(m)] \tag{2}$$

where ε_n is the atmosphere emissivity; m is the amount of the water vapor between the lower boundary of layer n and the height z; $(m + \Delta m)$ is the amount of the water vapor of the upper boundary of the layer n and the height z; T is the atmosphere temperature; σ is the Stefan–Boltzmann constant ($= 5.67*10^{-8}\ W/m^2K^4$).

All simulations were initialized at 06:00hr (UTC = +8), and ran for 13 h. Simulation results during 9:30–17:30hr were used for analysis. The minimal output interval was set as 10min, to be consistent with the mobile measurement interval.

Fig. 3. Showed the framework of this study: first, sensitivity analyses were conducted for the recent model updates; second, the optimal model in the sensitivity analyses was used for model evaluation regarding different GI typologies, output intervals, and thermal-radiative variables. The detailed experimental settings were illustrated in the following two sections.

Table 2
Meteorological conditions of three forcing schemes.

Meteorological parameters	Input value		
	Simple forcing	Full forcing	
		Cloud forcing	Radiation forcing
Air temperature (°C)	Daily max and min values	Daily half-hourly profile	Daily half-hourly profile
Relative humidity (%)	Daily max and min values	Daily half-hourly profile	Daily half-hourly profile
Wind speed (m/s)	Daily prevailing wind speed	Daily half-hourly profile	Daily half-hourly profile
Wind direction (°)	Daily prevailing wind direction	Daily half-hourly profile	Daily half-hourly profile
Solar factor/ Cloud/ Radiation	Solar factor adjustments (0.9, 0.8, 0.5)	Daily half-hourly profile (Medium clouds)	Daily half-hourly profile (Direct, diffuse radiations)
Soil initial temperature (°C)	Daily average value in different depth (upper, middle, deep and bedrock layers)	Daily average value in different depth (upper, middle, deep and bedrock layers)	Daily average value in different depth (upper, middle, deep and bedrock layers)
Soil humidity (%)	50, 55, 60, 60 (upper, middle, deep and bedrock layers)	50, 55, 60, 60 (upper, middle, deep and bedrock layers)	50, 55, 60, 60 (upper, middle, deep and bedrock layers)

2.4. Sensitivity analyses

To understand the effect of the input variations on the outputs of the model [52], sensitivity analyses were conducted. Specifically, four aspects were investigated for their impacts on the thermal-radiative outputs of ENVI-met:

1) The new radiation module Index View Sphere (IVS): IVS is a new advanced radiation transfer scheme, which allows a more detailed calculation of secondary radiative transfer. However, it costs higher RAM for computer equipment at exchange for higher accuracy. The sensitivity test aims to show whether the expected accuracy improvement is worth taking higher computer memory with IVS on;
2) Meteorological boundary conditions: the simple forcing and two full forcing (forced cloud and forced radiation) schemes were used and compared to evaluate the impacts of boundary condition settings;
3) Material characteristics of construction and plants: the default and localized settings were both applied to find out the necessity of customizing surface and plant properties for the local case;
4) The output intervals: three output timescales were used and compared in this study (i.e., 10min, 30min, and 1 h) to examine the reasonability of applying mobile measurement data to validate ENVI-met model.

To examine the above four aspects, an initial model was started with the default materials, IVS off, and simple forcing. The following models were built with one aspect changed in each run, while other aspects kept constant. The explicit steps and settings are shown in Table 3, where words in blue represent the changing setting.

2.5. Evaluated parameters and statistical metrics

After the sensitivity tests, the optimal model - LocalizedMaterials, was used for the evaluation analysis. Both thermal and radiative outputs of ENVI-met simulations were evaluated. Thermal parameters included air temperature (AT) and relative humidity (RH), while radiative parameters considered mean radiant temperature (MRT), downward and upward radiant fluxes, i.e., the downward shortwave and longwave fluxes (SW_{down} and LW_{down}), the upward shortwave and longwave fluxes (SW_{up} and LW_{up}), and wall-outgoing (LW_{out}) and wall-incoming (LW_{in}) longwave fluxes (mainly for green wall and bare wall points). Please see the illustration in Fig. 4.

Four statistical metrics were primarily adopted in this study for model evaluation: the coefficient of determination (R^2), the index of agreement (d), the root mean square error (RMSE) and its two elements (the systematic root mean square error (RMSEs), the unsystematic root mean square error (RMSEu)), and the mean bias error (MBE) [53]. These four metrics were selected based on the recommendations of Willmott [54,55], i.e., R^2 is an intuitive quantification to describe the model performance, d is complementary for R^2 to assess whether a model's predictions are error free; RMSE measures the average magnitude of the errors (non-negative).

In details, R^2 describes a goodness-of-fit measure for the variances between simulated and measured data, ranging from 0 to 1. d is a dimensionless index to indicate the ratio between the mean square error and the potential error, also ranging from 0 to 1 [54]. RMSE estimates the average magnitude of the errors, consisted of systematic and unsystematic errors: *RMSEs* and *RMSEu* [54]. *RMSEs* quantifies the systematic errors that occur consistently, while *RMSEu* describes the unsystematic errors that combined small effects into a constant [29]. MBE measures the average differences between the observations and estimations, which indicates whether the model overestimates (positive values) or underestimates (negative values) the observations [6]. Overall, higher reliability and accuracy of a model are associated with the conditions of: R^2 and d tending to be 1, RMSE and *RMSEs* closer to 0, *RMSEu* nearer to RMSE, and MBE nearer to 0. In addition, to compare

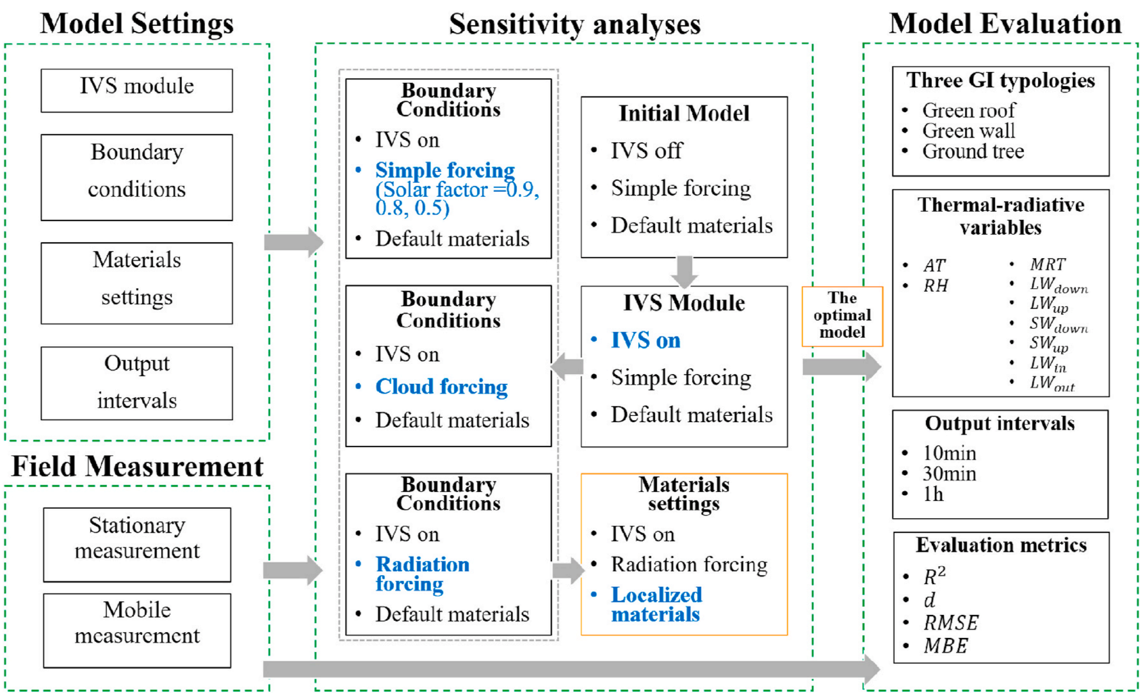

Fig. 3. Framework illustration of this study.

Table 3
Model settings and changes for each step.

No	Model Name	Settings			
		IVS Module	Meteorological Conditions	Materials	Output intervals
1	Initial Model	Off	Simple Forcing Solar Factor = 1	Default materials	10min, 30min, 1h
2	IVS on	On	Simple Forcing Solar Factor = 1	Default materials	10min, 30min, 1h
3	SolarFactor0.9	On	Simple Forcing Solar Factor = 0.9	Default materials	10min, 30min, 1h
4	SolarFactor0.8	On	Simple Forcing Solar Factor = 0.8	Default materials	10min, 30min, 1h
5	SolarFactor0.5	On	Simple Forcing Solar Factor = 0.5	Default materials	10min, 30min, 1h
6	CloudForcing	On	Full Forcing (Cloud inputs)	Default materials	10min, 30min, 1h
7	RadiationForcing	On	Full Forcing (Radiation inputs)	Default materials	10min, 30min, 1h
8	LocalizedMaterials	On	Full Forcing	Localized materials	10min, 30min, 1h

*Words in blue indicate the change step by step

the overall performance of different variables, RMSE and MBE of different variables were normalized to be NRMSE and NMBE by using the range of measured data as the denominator [38], so that the different variables with different units can be compared directly. These metrics were calculated through equations (3)–(7) [54,56].

$$d = 1 - \left[\sum_{i=1}^{N} (S_i - M_i)^2 \Big/ \sum_{i=1}^{N} \left(|S_i'| + |M_i'| \right)^2 \right] \tag{3}$$

$$RMSE = \left[RMSE_S{}^2 + RMSE_u{}^2 \right]^{1/2} = \left[N^{-1} \sum_{i}^{n} (S_i - M_i)^2 \right]^{1/2} \tag{4}$$

where:

$$RMSEs = \left[N^{-1} \sum_{i}^{n} \left(\widehat{S}_i - M_i \right)^2 \right]^{1/2} \tag{4a}$$

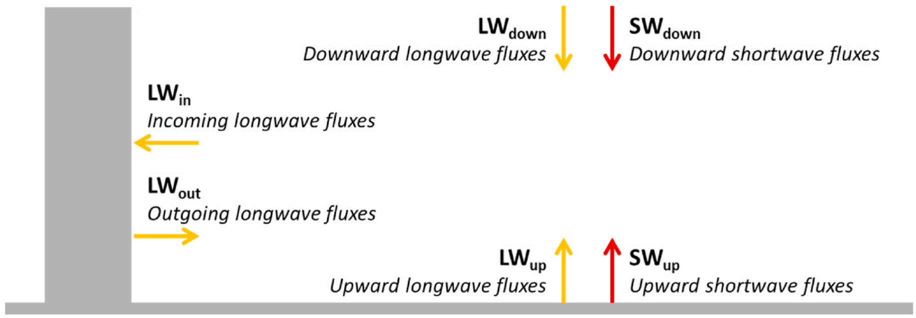

Fig. 4. Radiation fluxes direction illustration.

$$RMSEu = \left[N^{-1}\sum_{i}^{n}\left(S_i - \widehat{S}_i\right)^2\right]^{1/2} \tag{4b}$$

$$MBE = N^{-1}\sum_{i}^{n}(S_i - M_i) \tag{5}$$

$$NRMSE = RMSE / (M_{max} - M_{min}) \tag{6}$$

$$NMBE = MBE / (M_{max} - M_{min}) \tag{7}$$

where $S_i' = S_i - \overline{M}$, $M_i' = M_i - \overline{M}$, and $\widehat{S}_i = a + b^* M_i$; S_i is the simulation value by ENVI-met; M_i represents the measurement value; N denotes number of the data; $\overline{M}$ represents the mean of the measurement value; M_{max} is the maximum of the measurement value; M_{min} describes the minimum of the measurement value.

3. Results

The simulation results of the 11th Sep 2019 was briefly reported for two reasons: the weather on this day is a typical summer day in HK with partially cloudy weather conditions [15]; and the model performance on this day was better compared with other three measurement days.

3.1. Sensitivity analysis results

3.1.1. By different settings

In this section, eight models with different settings (see Table 3 for details) were investigated. With updating settings for each model, the impact of the settings can be evaluated. To cross-compare the average performance for all microclimate variables and locations, four dimensionless metrics were used, including R^2, d, NRMSE, and NMBE.

As shown in Fig. 5, the model performance was improved as the model settings got updated from the first to the final one (Localized materials), irrespective of output intervals and evaluation metrics.

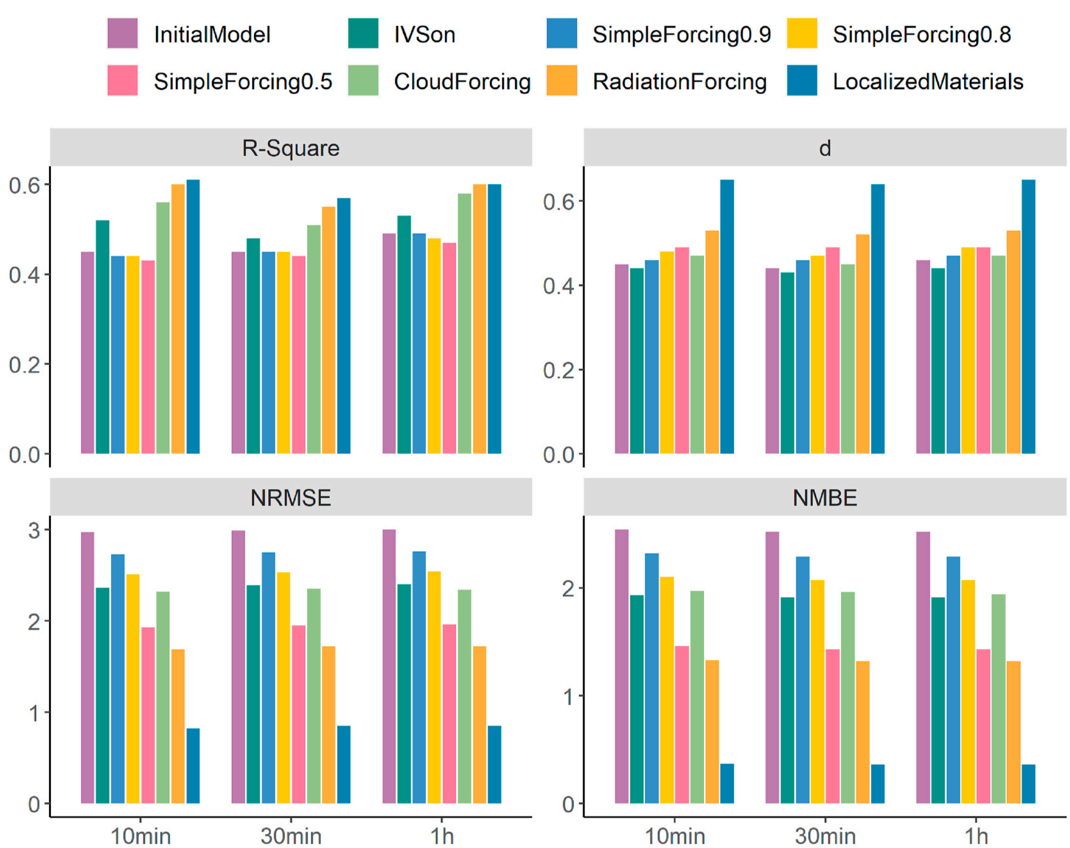

Fig. 5. Overall model performance by eight settings.

Specifically, the simple forcing with the adjusted solar factors (1, 0.9, 0.5) showed trivial differences based on R^2 and d. However, lower solar factors lead to smaller prediction errors and bias (NRMSE and NMBE). We also found that the cloud forcing model improved prediction accuracy based on R^2, yet deteriorated for other metrics – d, NRMSE, and NMBE. Despite above non-identical evidence, the most efficient settings to improve the model performance were by radiation forcing and localizing materials.

3.1.2. By different variables

Fig. 7 revealed the impacts of model settings on different thermal-radiative variables. SW_{down} was not included here, as it showed high deviation in RMSE and thus covered detailed differences of remaining variables (please see Figs. S2–1 in the supplementary file S2).

Generally, the prediction accuracy was improved for most of the variables from the initial to the final model. However, the prediction accuracy differed among the variables (shown in Fig. 6). For instance, variables with the best and stable estimation differ according to four evaluation metrics: MRT based on R^2, AT based on d and RMSE, and AT and RH based on MBE. Across different settings, R^2 of AT was observed to improve from 0.4 to 0.6; SW_{up} estimation was observed to be less accurate with IVS on and full forcing, showing the relatively higher RMSE and MBE; SW_{down} (Figs. S2–1) fluctuated minorly based on R^2 and d, but improved highly based on RMSE and MBE. Output interval rarely impact the patterns, except with MBE where 30 min interval had a lower MBE value than that of 10min and 1 h. The detailed metric values could be found in Tables S2–1.

3.1.3. By different points

This section uncovered the impacts of model settings on different locations: green roof (GR), bare roof (BR), green wall (GW), bare wall (BW), ground tree (GT), tree free (TF). Similar with Section 3.1.1, four dimensionless metrics were used including R^2, d, NRMSE and NMBE. Overall, almost all points reached the best performance in the final model (Localized materials), with smaller errors, lower biases, regardless of temporal scales. Besides, the model performance in the six points is sensitive to the evaluation metrics (see Fig. 7). Specifically, based on R^2, the range was 0.40–0.75; six sites showed little variation among the

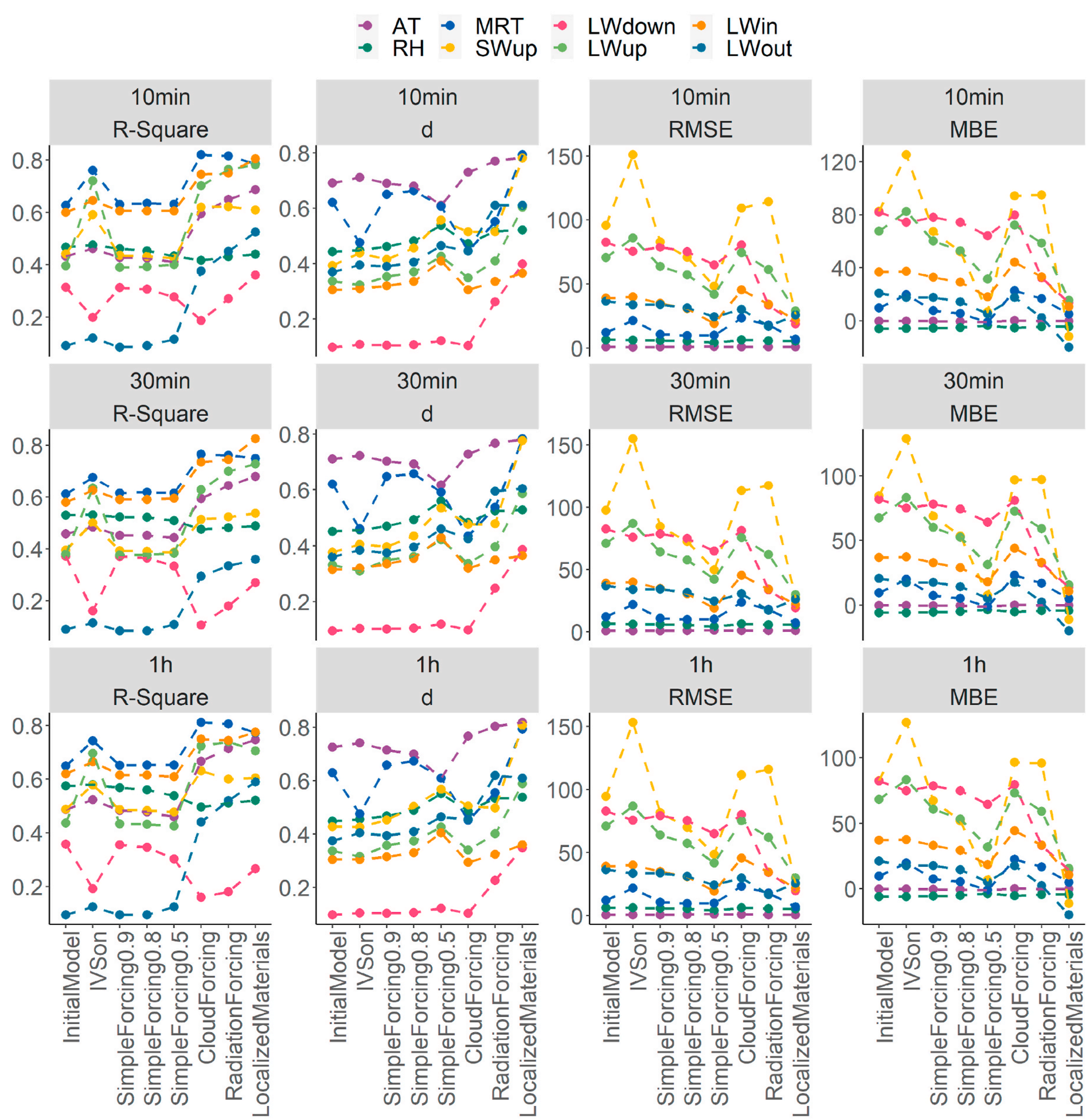

Fig. 6. Overall model performance by eight variables (*unit of RMSE and MBE: °C for AT, MRT; % for RH, W/m² for radiation fluxes*).

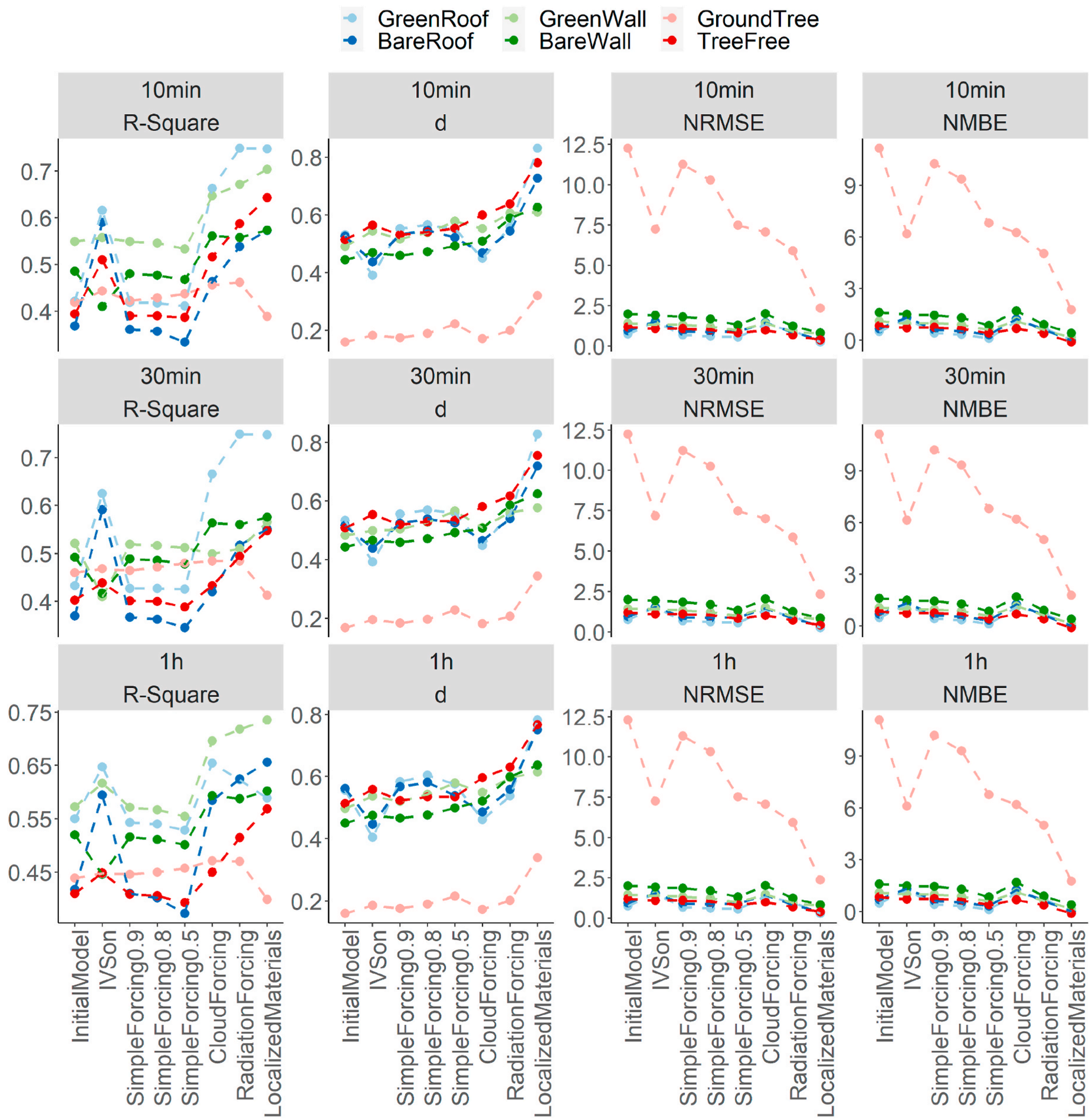

Fig. 7. Overall model performance by six points.

three simple forcing models, while the performance improved apparently in two full forcing models (forced cloud and radiation). Using d, six locations presented similar values except for GT site that showed relatively low values from 0.2–0.4. In terms of the error-based metrics, NRMSE, and NMBE, all sites almost showed insensitive to the chosen model settings, except at GT point had the improved performance in IVS on, full forcing and localized materials models.

Given the results in this section, the optimal model was the Localized materials, which was henceforth selected to evaluate the thermal-radiative performance of ENVI-met. The next two sections mainly discussed nine thermal-radiative variables given their significances in both outdoor thermal comfort and building energy performance. Model developers and users can further understand the simulation deviations based on the detailed illustrations below.

3.2. Evaluation in thermal variables

3.2.1. Air temperature

Across three output intervals and six points, the performance of ENVI-met in AT was averagely described by $R^2 = 0.70$, d = 0.79, RMSE = 0.91 °C, and MBE = −0.15 °C. The output intervals did not impact this observation, with slightly better performance for 1 h interval and relatively inferior for 30min ($R^2 = 0.75$ vs. 0.68, d = 0.82 vs. 0.78, RMSE = 0.83 vs 0.97 °C). AT was slightly underestimated in three output intervals (MBE = −0.16 ~ −0.13 °C). Detailed values were reported in Tables S2–2.

A point-by-point analysis indicated higher variability (see Fig. 8). R^2 achieved high as 0.90 at GW and relatively lower at BR and TF (0.55). With d, a range of 0.67–0.91 was observed, highest at BW and lowest at BR. The least error was found at BW (RMSE = 0.54 °C), while the largest error was observed at BR (RMSE = 1.77 °C). The results also showed that ENVI-met tended to underestimate AT at the two rooftop sites (MBE = −0.39 °C and −1.46 °C for GR and BR) and BW (MBE = −0.17 °C), but overestimated AT near GI at pedestrian level (MBE = 0.34 °C for GW and 0.76 °C for GT). TF site had the least MBE nearest to zero (0.04 °C).

It is important to mention that the interpretations for the above values should consider the accuracy of the measurement equipment (HOBO sensor in this study, ±0.3 °C), as some prediction deviations may

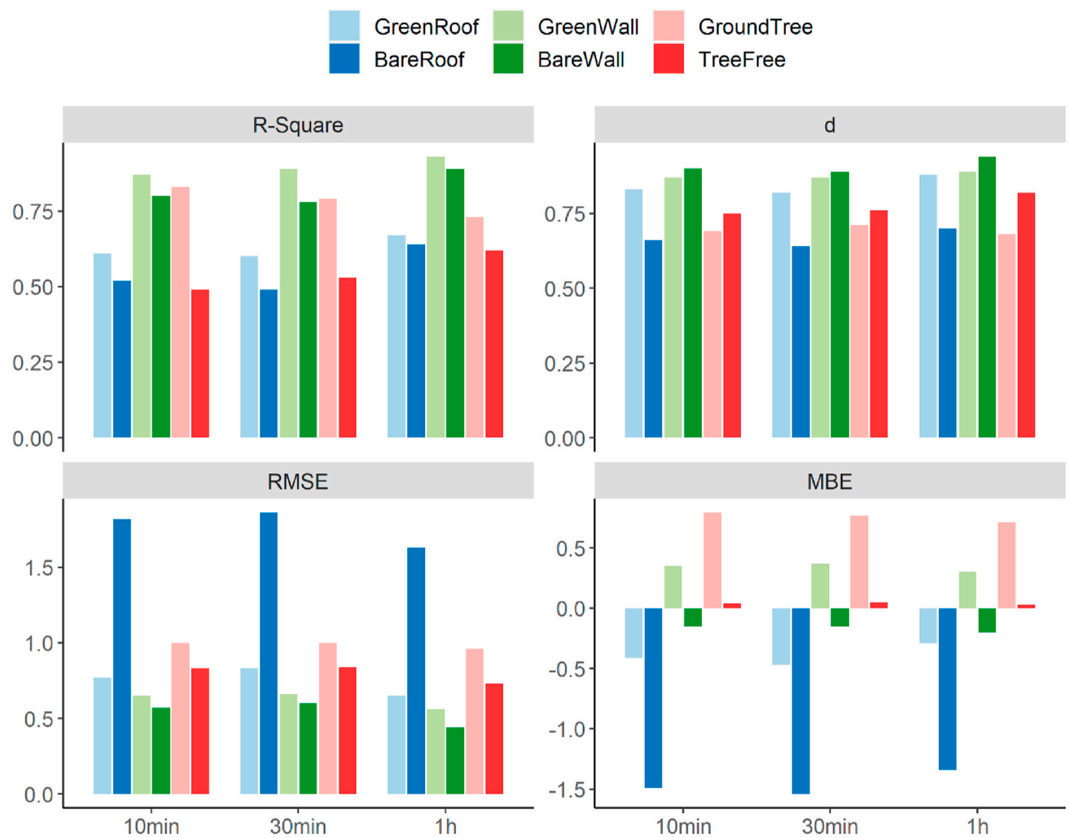

Fig. 8. Four evaluation metrics in AT (unit of RMSE and MBE: °C).

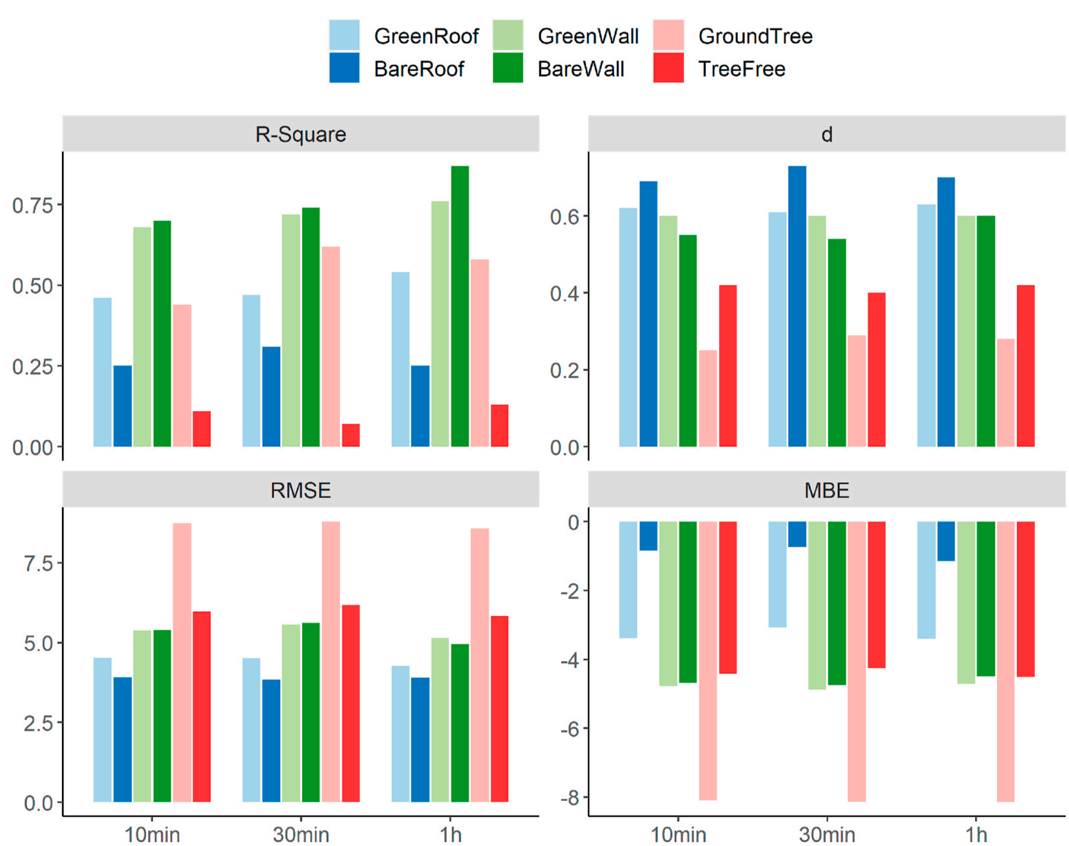

Fig. 9. Four evaluation metrics in RH (unit of RMSE and MBE: %).

arise from the measurement errors. The results indicated that ENVI-met has potential limitations to estimate AT in higher z-level grids, as the AT predictions at roof sites showed high deviations relative to observations at roof-level.

3.2.2. Relative humidity

Irrespective of the output intervals and sites, the overall performance of ENVI-met for RH estimation was averaged $R^2 = 0.48$, $d = 0.53$, RMSE = 5.62%, and MBE = −4.36%. Three output intervals presented small variations: better performance presented by 1 h interval, while the slightly inferior by 10 min ($R^2 = 0.52$ vs. 0.44, d = 0.54 vs. 0.52, RMSE = 5.45 vs. 5.65%). ENVI-met underestimated RH at three output intervals (MBE = −4.40 ~ −4.30%). The detailed values were summarized in Tables S2–3.

For location specific analysis, the model performance shows variability depending on the evaluation metrics (see Fig. 9). R^2 reached the highest at BW (0.77) and the lowest at TF (0.10). d was high as 0.71 at BR, but low as 0.27 at GT. The estimation error was maximum at GT (RMSE = 8.70%) and minimum at BF (RMSE = 3.88%). ENVI-met underestimated RH in all points, with MBE ranging from −0.91% ~ −8.12% (BF ~ GT).

Given the sensor accuracy of HOBO was ±2.5%, ENVI-met performed well in RH estimation, except near GT. The deviation can be partly attributed to weather condition. We collected data during a typical summer day in HK, with partially cloudy conditions. One study conducted in similar hot-humid subtropical climate found that fully cloudy weather lead to distinct discrepancy in water vapor fluxes estimation [31].

3.3. Evaluation in radiative variables

3.3.1. Mean radiant temperature

For all output intervals and sites, the average performance in MRT was described by $R^2 = 0.77$, d = 0.79, RMSE = 7.07 °C, and MBE = 4.96 °C. The differences of three output intervals were insignificant. 10min showed the highest d (0.79) and R^2 (0.79), with a relatively low RMSE (6.99 °C); 30min performed moderately lower d (0.78) and R^2 (0.75), higher RMSE (7.12 °C). MRT was overestimated for three output intervals, with MBE = 4.89–4.99 °C. The detailed values were given in Tables S2–4.

Concerning the location-related differences, inconsistences were observed (see Fig. 10). R^2 showed that TF had the highest value (0.87) whereas BW presented the lowest value (0.62). Based on d, except for GT with a low value as 0.37, other five sites presented 0.81 or even higher. The smallest error was presented in GT and TF sites (RMSE = 5.79 and 5.57 °C respectively), while largest error was found in GW (RMSE = 8.61 °C). According to MBE values, MRT was overestimated for all six points, ranging 1.28–7.81 °C (BW ~ GW).

Although six-directional method is widely identified as the most accurate approach for MRT measurement [57,58], the systematic errors arising from the sensors and the unsystematic errors related with experimental operation should also be considered when interpreting the above results.

3.3.2. Down- and upward fluxes

Shortwave fluxes

Downward shortwave radiation

In ENVI-met, downward shortwave radiation (SW_{down}) is the aggregation of diffuse shortwave radiation from sky, reflected shortwave radiation from surrounding environment, and incoming direct shortwave radiation [7]. Generally, the overall performance of SW_{down} was: moderate variance ($R^2 = 0.52$), decent agreement (d = 0.74), low bias (MBE = −18.96 W/m^2), but large deviation (RMSE = 220.44 W/m^2). Different output intervals showed minor discrepancies, 10min performed better than 30min with $R^2 = 0.55$ vs. 0.50, d = 0.75 vs. 0.73, and RMSE = 220.44 vs. 212.19 W/m^2. SW_{down} was underestimated

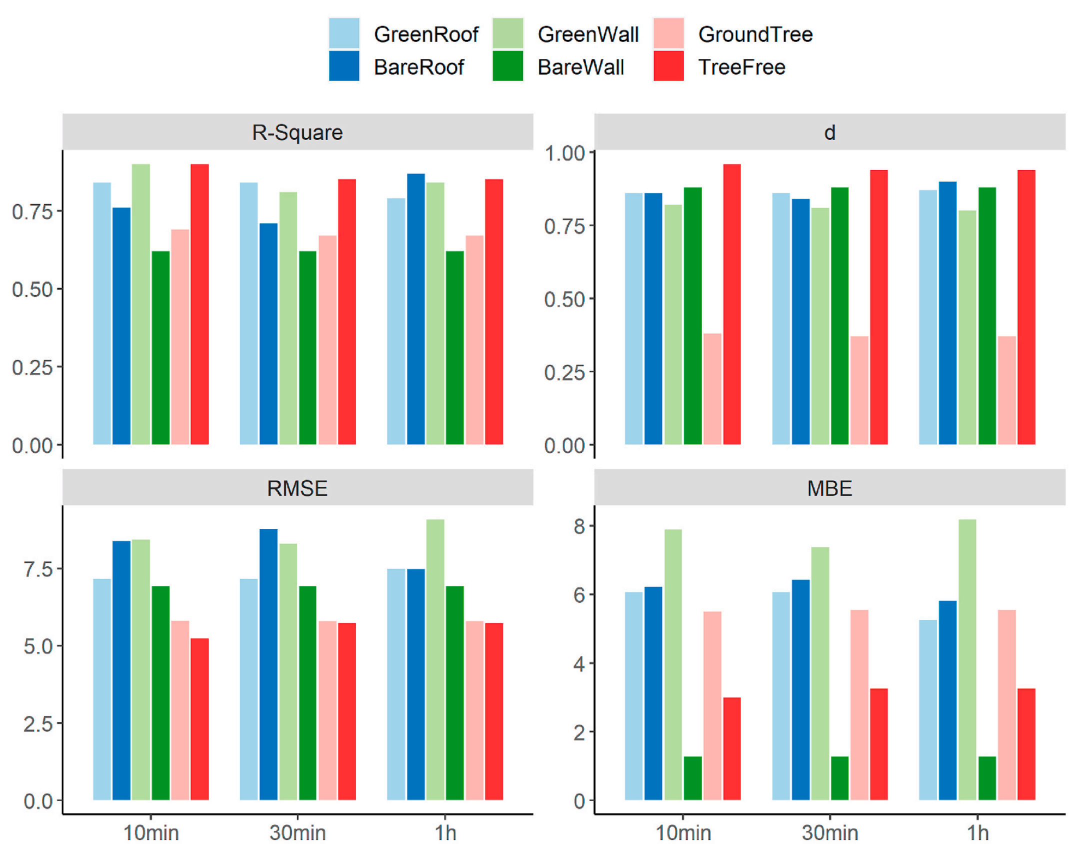

Fig. 10. Four evaluation metrics in MRT (unit of RMSE and MBE: °C).

marginally (MBE = −29.39 ~ −12.71 W/m^2) for three intervals. The details were shown in Tables S2–5.

The differences among the six sites were rather complex. Quantified by R^2, TF yielded better performance (0.86), whereas BW and GW showed inferior performance (0.13 and 0.25 respectively) (see Fig. 11). Higher d was found at BR (0.93) and TF (0.95), while the lowest at GT (0.32). Two wall points presented large errors (RMSE = 363.67 and 436.68 W/m^2 for GW and BW) and underestimated bias (MBE = −175.77 and −231.70 W/m^2). At the other four sites, RMSE ranged 41.73–191.65 W/m^2 (GT ~ GR). Besides, there was moderately overestimation at the roof sites (MBE = 132.01 and 85.62 W/m^2 for GR and BR) and slight overestimation at GT and TF (MBE = 32.94 and 43.14 W/m^2).

There are several possible reasons to explain the discrepancies of SW_{down} estimation. As this study applied mobile measurement to collect radiative variables, unsystematic errors due to operations should be considered. The shading discrepancy was also reported in a previous study to explain the errors of radiative variables estimation [33]. Besides, SW_{down} is highly sensitive to building geometry in ENVI-met. This study collected the wall sites data near an arc-shaped wall. Although the model mimicked the reality to the utmost, shading errors may lead to large deviations of SW_{down} estimation. Furthermore, calculating shortwave fluxes requires segregating global solar radiation into direct and diffuse components accurately [59], which potentially brings some prediction deviations.

Upward shortwave radiation

ENVI-met predicted upward shortwave radiation (SW_{up}) by calculating the fraction of ground reflected shortwave radiation over the overall incoming shortwave radiation [7]. Throughout all output intervals and points, SW_{up} was predicted reasonably with averaged R^2 = 0.58, d = 0.79, RMSE = 26.25 W/m^2, and MBE = −11.37 W/m^2. Minor differences were found among three output intervals, but 1 h outperformed in d = 0.81, R^2 = 0.61, and RMSE = 25.31 W/m^2. Tables S2–6 showed other details.

Fig. 12 showed the performances for six locations, with the highest R^2 in GR (0.80), the best d in two roof points (0.91) and TF (0.92). GT showed the lowest error and bias (RMSE = 5.98 W/m^2 and MBE = 4.02 W/m^2), yet the lowest R^2 = 0.05. Furthermore, ENVI-met tended to underestimate SW_{up} in GR (MBE = −11.00 W/m^2), two wall points (−17.31 and −39.33 W/m^2 for GW and BW), and TF (−5.34 W/m^2), but overestimate SW_{up} marginally in GT (4.02 W/m^2). MBE of BR was close to zero (0.75 W/m^2).

With IVS scheme on, ENVI-met no longer estimated SW_{up} based on domain-wide mean albedo like previous versions, which largely improved the estimation performance [60]. However, the intra-domain prediction deviations for multiple points are worth attention.

Longwave fluxes

Downward longwave radiation

In ENVI-met, downward longwave radiation (LW_{down}) consisted of emitted radiations from the sky, surrounding vegetation and buildings, as well as reflected radiations from buildings. Overall, for all output intervals and points, LW_{down} estimation was measured by relatively low d (= 0.38) and R^2 (= 0.30), low error (RMSE = 19.34 W/m^2) and bias (MBE = 13.89 W/m^2). Trivial variances were found for three output intervals: 10min yielded better performance with higher R^2 (0.36) and d (0.40), lower MBE (13.68 W/m^2), while 1 h underperformed with a marginally higher error (RMSE = 19.78 W/m^2) and bias (MBE = 14.27 W/m^2). Remaining details were revealed in Tables S2–7.

About six sites (shown in Fig. 13), ENVI-met underpredicted LW_{down} for TF site (MBE = −10.03 W/m^2), while overpredicted LW_{down} for the remaining five sites (MBE = 0.64–30.71 W/m^2). The implications of R^2 and other three metrics were reverse for BR, GW, and TF points. For example, GW showed a reasonable R^2 (0.65), yet relatively low d (0.23); BR had a relatively high d (0.41), but low R^2 (0.11).

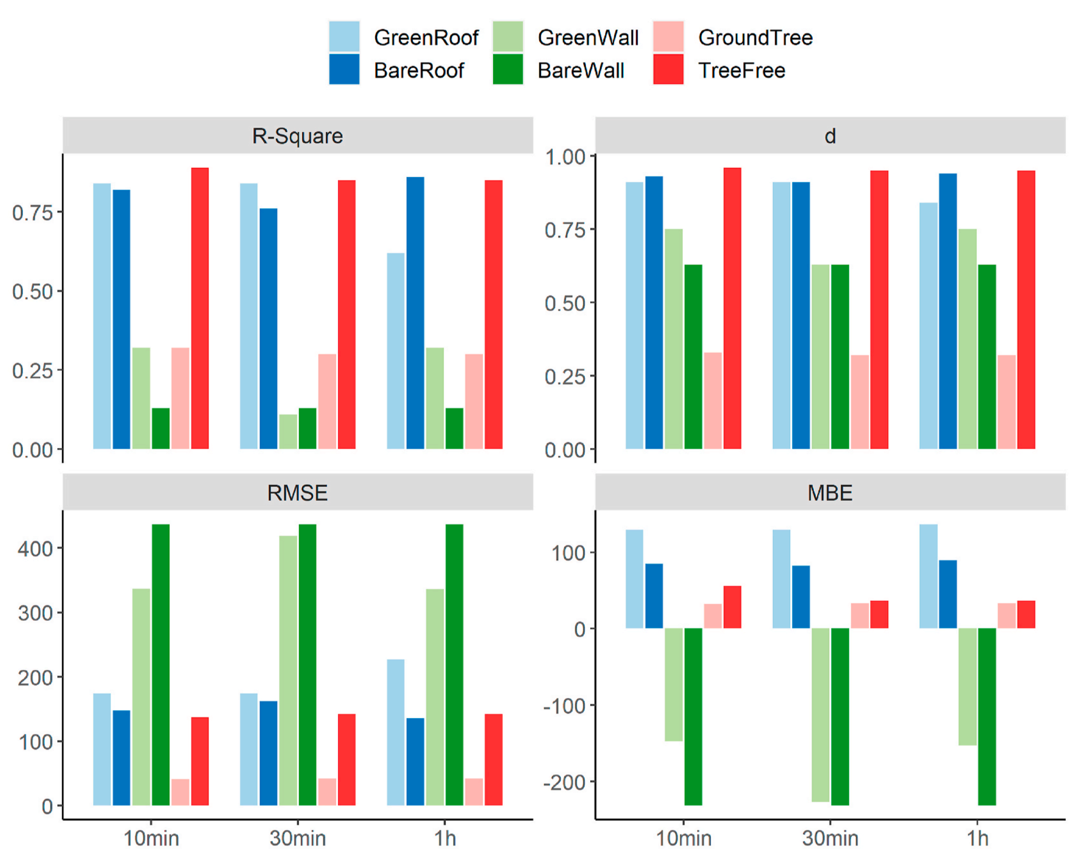

Fig. 11. Four evaluation metrics in SW_{down} (unit of RMSE and MBE: W/m^2).

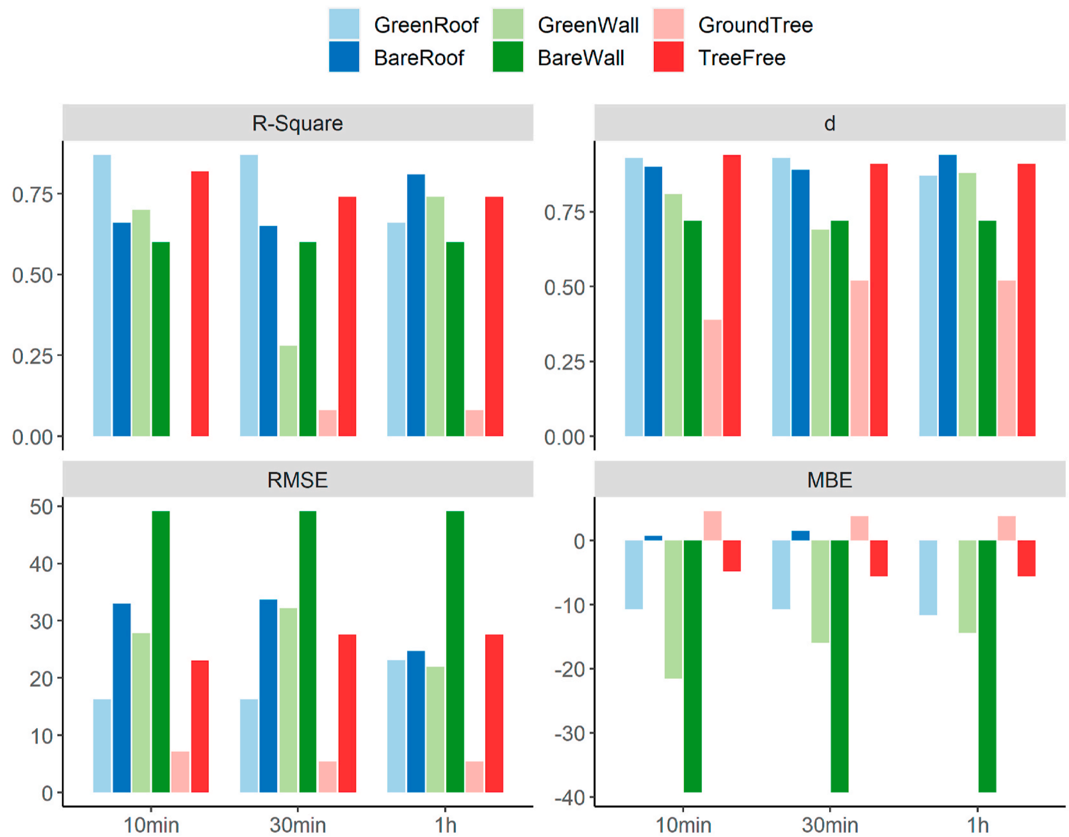

Fig. 12. Four evaluation metrics in SW_{up} (unit of RMSE and MBE: W/m^2).

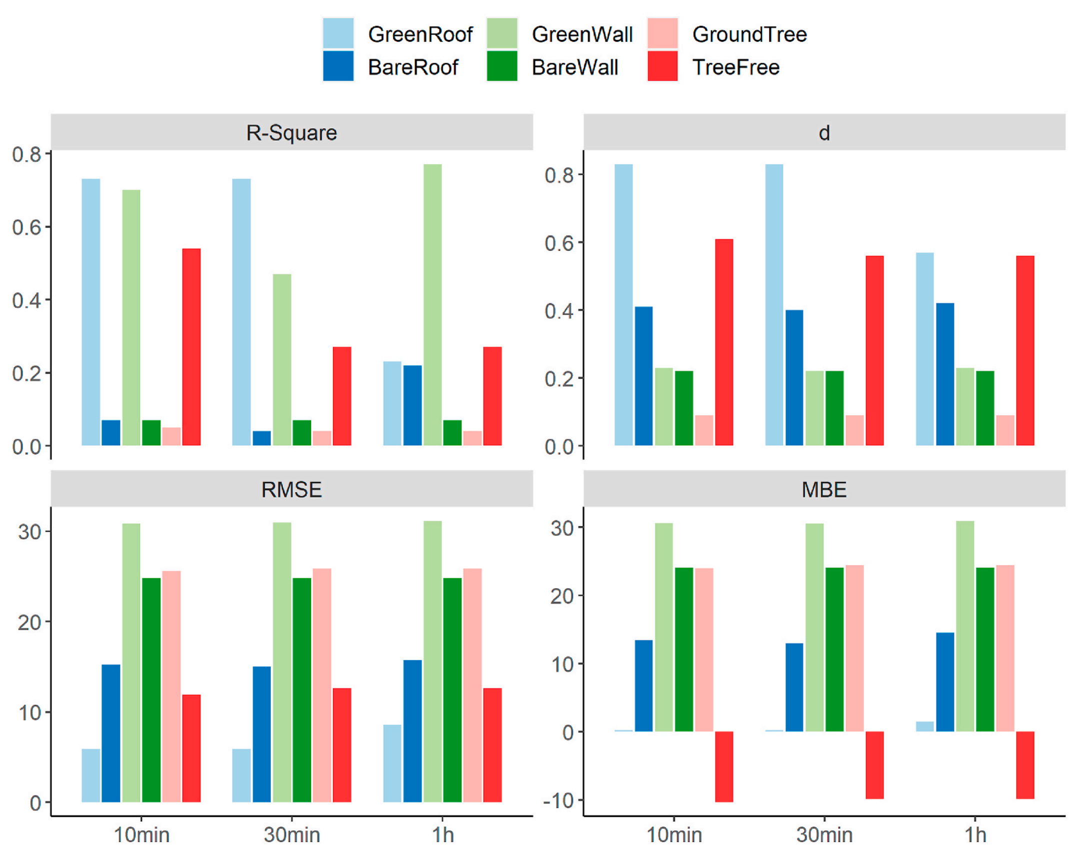

Fig. 13. Four evaluation metrics in LW_{down} (unit of RMSE and MBE: W/m^2).

The rather poor estimation of LW_{down} in two wall points can also be attributed to the arch-shaped wall described in Section 3.3.2 already. The deviations of LW_{down} in ground tree were partially explained by the shading effects of the canopy and surrounding buildings, estimation errors of leave surface temperature, and imperfect tree shape modelling and LAD values.

Upward longwave radiation

Upward longwave radiation (LW_{up}) was mainly dependent on the ground emitted radiations [17]. For all output intervals and sites, LW_{up} was reasonably predicted with $R^2 = 0.74$, d = 0.59, RMSE = 29.68 W/m^2, and MBE = 15.53 W/m^2. As for output intervals, 10min outperformed with highest R^2 (0.78) and d (0.60), and lowest RMSE (29.07 W/m^2), while 1 h showed the lowest MBE (15.45 W/m^2). Complete values were presented in Tables S2–8.

Concerning six points, BR presented the highest R^2 (0.92), when GR outperformed with the highest d (0.83), lowest error (RMSE = 14.03 W/m^2) and bias (MBE = 11.15 W/m^2). As depicted in Fig. 14, GW showed the largest errors (RMSE = 42.87 W/m^2) and highest bias (MBE = 41.62 W/m^2) among the six sites. Besides, GT showed a lowest d (0.11) and R^2 (0.39). ENVI-met underestimated LW_{up} at BR (MBE = −32.27 W/m^2), and overestimated LW_{up} in the remaining sites with MBE = 11.15–41.62 W/m^2. Three output intervals for six points demonstrated almost consistent performances, except in TF. TF outperformed in 10min with larger R^2 and d, and lower RMSE and MBE.

ENVI-met V4.4.6 estimated the upwelling longwave fluxes based on the seen view facets through IVS scheme, rather than the average surface temperature in the domain in the previous versions [60]. This apparently improved the LW_{up} radiation estimation, compared with previous study [33].

3.3.3. Incoming and outgoing longwave fluxes near walls

Incoming longwave fluxes

Incoming longwave radiation (LW_{in}) involves the longwave radiation emitted by atmosphere and vegetation, and reflected by surrounding buildings towards the walls [7]. Summarizing all output intervals and wall points, LW_{in} was estimated with high R^2 (0.80) and moderate d (0.36), low errors (RMSE = 21.74 W/m^2) and bias (MBE = 10.61 W/m^2). Regarding output intervals, little difference was found, especially between 10min and 1 h: $R^2 = 0.81$ vs. 0.78, d = 0.37 vs. 0.36, RMSE = 21.74 vs. 21.71 W/m^2, and MBE = 10.62 vs. 10.69 W/m^2. Other details were shown in Tables S2–9.

For two wall points, R^2 was high (0.72 and 0.88 for GW and BW, respectively) (see Fig. 15). Irrespective of output intervals, BW presented a higher d than GW (0.48 vs. 0.25), while GW outperformed with a lower RMSE (10.43 vs. 33.05 W/m^2). Moreover, ENVI-met tended to overestimate the LW_{in} near BW (MBE = 31.25 W/m^2) and underestimate LW_{in} the near GW (MBE = −10.02W/m^2).

Outgoing longwave fluxes

Outgoing longwave fluxes (LW_{out}) represent the longwave radiation emitted and reflected by the walls towards the atmosphere. Across all output intervals and wall points, LW_{out} averagely presented low R^2 (0.49), reasonable d (0.61), RMSE (25.96 W/m^2) and MBE (−19.82 W/m^2). The differences among output intervals were insignificant: the same value of d (0.61), RMSE = 25.83–26.07 W/m^2, MBE = −19.87 ~ −19.75 W/m^2, while R^2 showed moderately larger range at 0.36–0.59. See Tables S2–10 for details.

Regarding two wall points, similar with LW_{in}, d was lower for GW and higher for BW (0.38 vs. 0.84), which was consistent for three output intervals (see Fig. 16). BW presented a slightly higher R^2 than GW (0.51 vs. 0.47), yet had a lower RMSE (10.98 vs. 40.94 W/m^2). ENVI-met overestimated LW_{out} for both wall sites, with MBE = −0.74 ~ −38.90 W/m^2 for BW ~ GW.

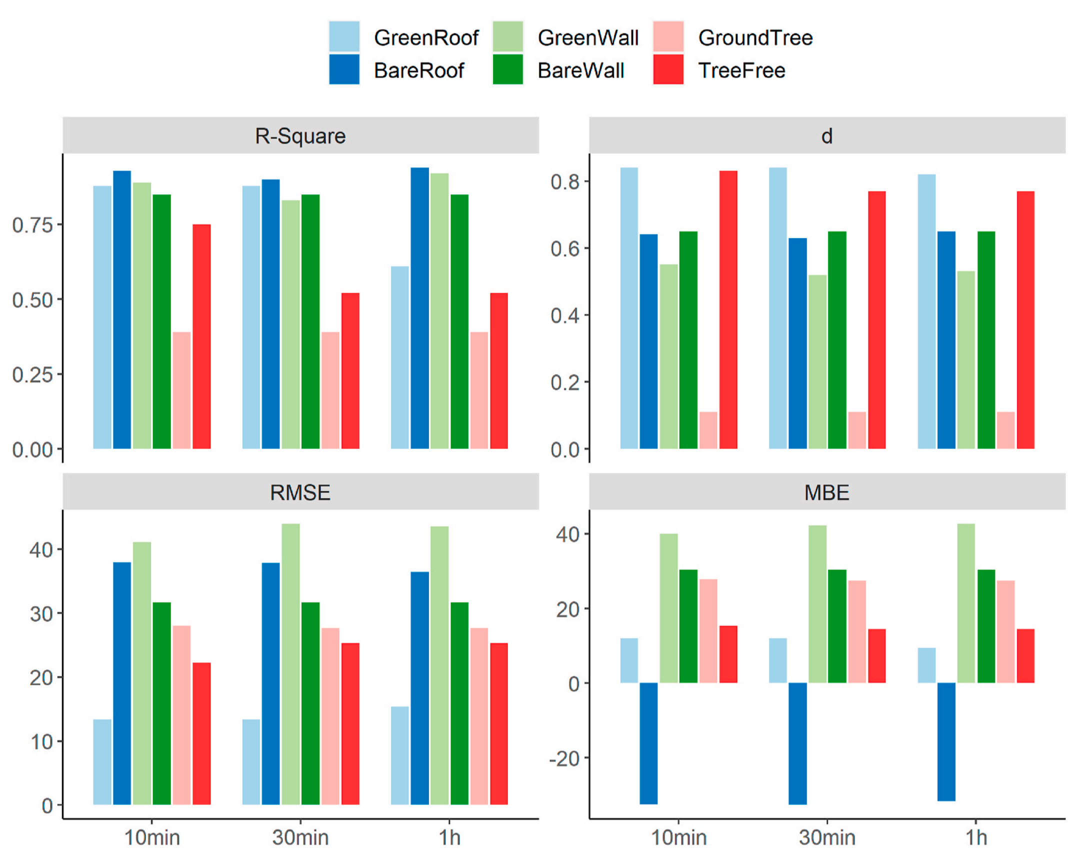

Fig. 14. Four evaluation metrics in LW_{up} (unit of RMSE and MBE: W/m^2).

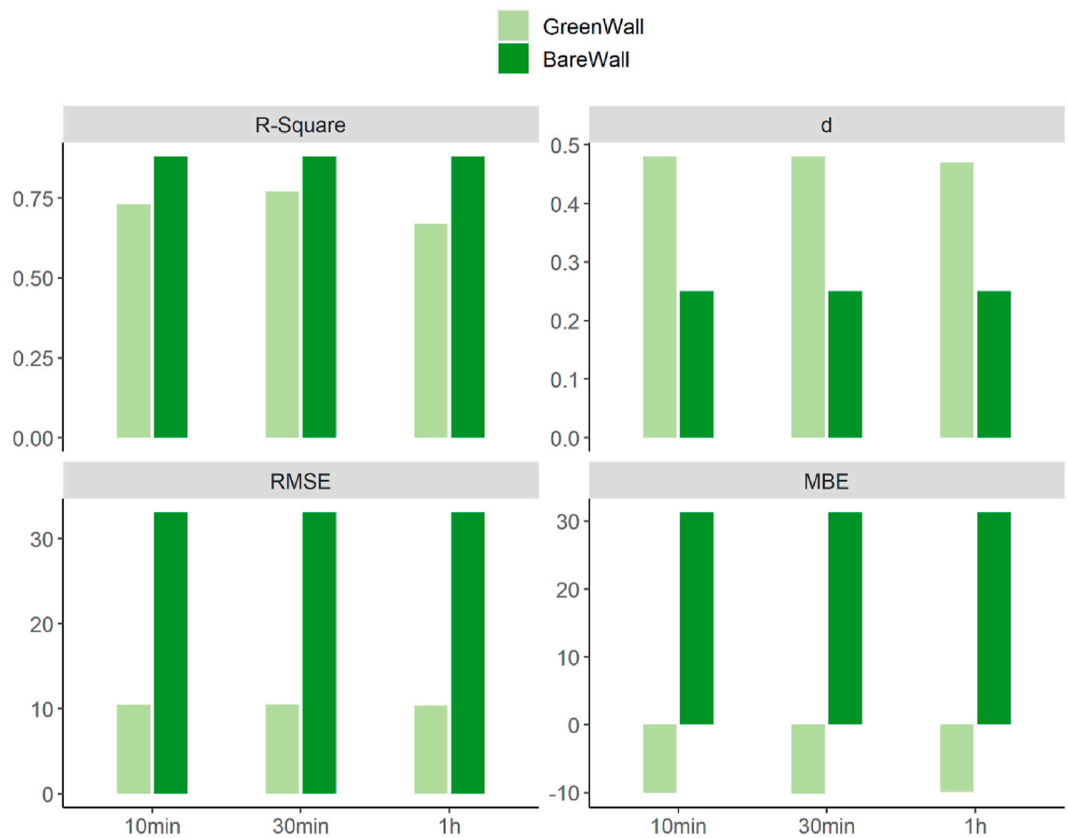

Fig. 15. Four evaluation metrics in LW_{in} (unit of RMSE and MBE: W/m^2).

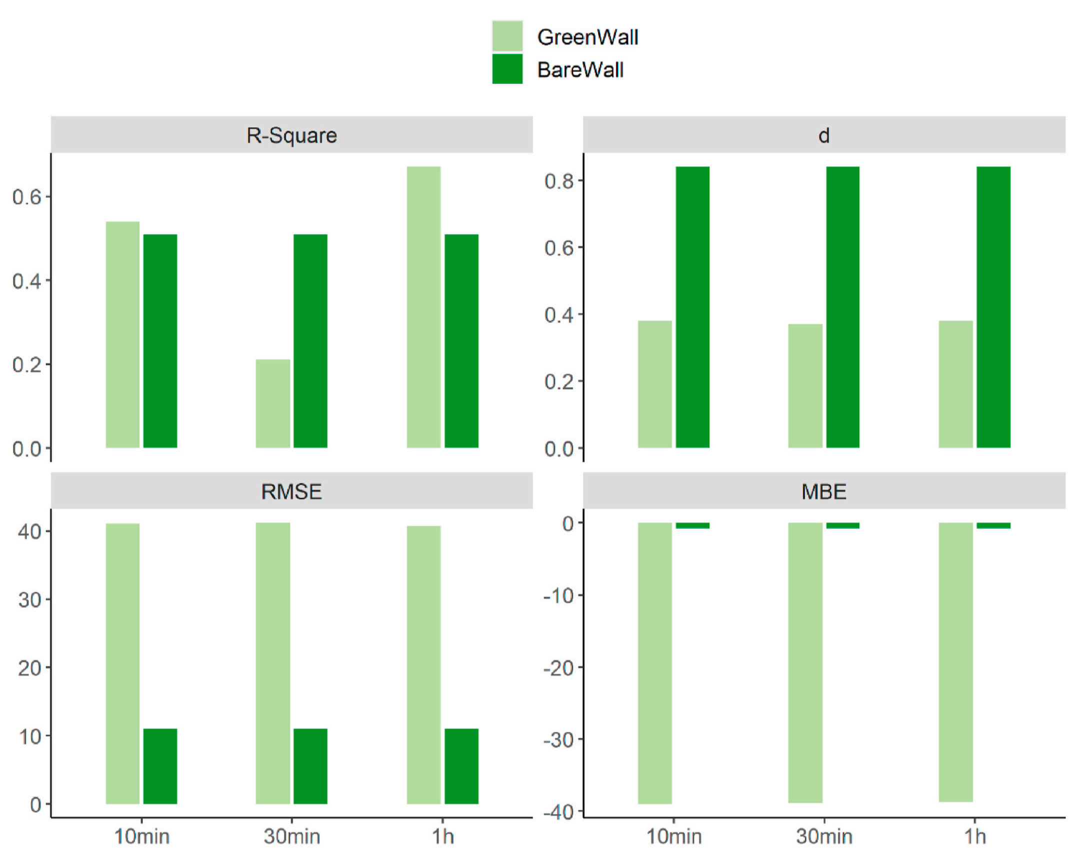

Fig. 16. Four evaluation metrics in LW_{out} (unit of RMSE and MBE: W/m^2).

4. Discussion

4.1. ENVI-met performance and evaluation metrics

According to previous studies of ENVI-met evaluation, as summarized in Appendix Table A1, thermal variables were investigated mostly. AT was evaluated in all listed studies and generally performed reasonably with high R^2 and low errors. Humidity was quantified by different variables, i.e., relative humidity, absolute humidity, and specific humidity, which makes inter-comparison an intricate task. Radiative variables, especially longwave and shortwave fluxes in different directions, were less investigated. MRT, as a significant variable for outdoor thermal comfort, showed larger variations than AT and RH. One possible reason is that MRT fluctuates widely towards solar radiation and the surrounding environment, which may not be explicitly mimicked by ENVI-met, especially when a coarse model is compared with a finer reference data [33].

This study evaluated and compared the thermal-radiative performance of ENVI-met in six points, including three GI typologies and corresponding reference sites. The results indicated that the prediction capability of ENVI-met varied among different variables and sites. For different variables, ENVI-met performed better in estimating thermal variables with average R^2 (0.70 and 0.48 for AT and RH) and d (0.79 and 0.53 respectively), low errors (RMSE = 0.91 °C and 5.62% respectively) and bias (MBE = −0.15 °C and −4.36% respectively). The performance of radiative variables was not consistent. As MRT was most accurately estimated (R^2 = 0.77, d = 0.79, RMSE = 7.07 °C, MBE = 4.96 °C), SW_{down} was estimated with the largest deviations with R^2 = 0.52, d = 0.74, RMSE = 220.44 W/m^2, MBE = −18.96 W/m^2. Concerning six sites, ENVI-met responded differently, i.e., ground or roof level, with or without greening, with different GI typologies. Two roof points exerted higher errors than ground sites when estimating AT and MRT (RMSE = 0.75–1.77 °C for AT, 7.27–8.22 °C for MRT, all above the average values). Current literature scarcely provided similar evidence supported by measurement data, a study validated ENVI-met and found slightly lower errors than our study (RMSE = 1.07–1.21 °C for AT, 4.27–6.13% for RH) [20], see in Appendix Table A2. One parametric study without field measurement claimed that ENVI-met should be used with caution for roof-level mitigation strategies [61]. The reason lies in the grid-dependence at roof level, so that errors and uncertainties were introduced albeit less than the effects of mitigation strategies. This partly explained the large errors at roof level observed in our study, as in ENVI-met, the grid resolution at roof level cannot be refined into five sub-grids like the lowest cell on ground level. Regarding wall points, compared with a previous study that measured both bare and green walls and then evaluated the simulation results [32], our study revealed similar error range in MRT (RMSE = 6.93–8.61 °C vs. 7.98–8.30 °C for our study and reference study respectively), but smaller deviations in LW_{down} (24.79–30.98 W/m^2 vs. 115.27–209.60 W/m^2) and SW_{up} (27.30–49.08 W/m^2 vs. 61.86–87.12 W/m^2). These values indicated that the MRT discrepancies in our study mainly came from solar radiation deviations, while the solar radiation errors arose from the complex geometry of walls, as well as the mismatch between coarse model and finer reference data, which has been explained in section 3.3.1. In terms of ground points with and without trees, our study revealed smaller error ranges than related studies [4,26,30,31,33]. Involving new ACRT module, TF site in our study performed better than similar site in another study in subtropical climate background, with the errors of AT (RMSE = 0.80 vs. 1.13 °C in our study and reference study) and SW_{down} (RMSE = 140.36 vs. 185.52 W/m^2). Moreover, GT site showed much better results. Comparing with studies in subtropical humid climate and arid climate [26,31], our study showed smaller errors in AT (RMSE = 0.99 °C vs. 3.97 °C for our study and reference study respectively), MRT (RMSE = 5.79 °C vs. 10.97–18.13 °C), and SW_{down} (RMSE = 41.73 vs. 242.15 W/m^2). This indicates the new Advanced Canopy Radiation Transfer (ACRT) module improves the estimations of microclimate parameters in canopies [62].

Concerning evaluation metrics, some studies only used R^2 for model evaluation and validation [13,16,17,59,63–66]. Our study revealed variable results by different evaluation metrics, which indicated that single evaluation metric may limit our overall understanding of the model performance. In accordance with the suggestions in previous studies [54,56,67], we underscored the necessary to apply multiple metrics for model evaluation and validation in the future.

4.2. Recent updates of ENVI-met and importance of localized settings

To evaluate recent updates of ENVI-met, this study compared the impacts of different model settings on the model performance of ENVI-met, including four aspects: IVS module, meteorological boundary conditions, materials, and output intervals. Our results indicated that the newly implemented IVS scheme yielded higher accuracy and faster speed at the cost of higher requirement in RAM requirement. It significantly decreased the errors of radiation fluxes in $SW_{down,}$ LW_{down}, and LW_{out}, especially for GW and GT sites. Besides, we found that radiation forcing and localized materials settings are essential to improve the overall model performance. Since radiation forcing requires detailed information in direct and diffuse radiations, simple forcing scheme with adjusted solar factors or cloud forcing with cloud amounts (in oktas unit) is usually an alternative in previous studies. However, our study found that solar factor adjustment in simple forcing may improve the performance in some variables, i.e., SW_{up}, SW_{down}, and LW_{in}, but decreased the estimation accuracy in AT. This was also discussed in a previous study that solar factor adjustment has both conceptual and implementation limitations [33]. Cloud forcing performed better than simple forcing with adjusted solar factors, yet inferior to the radiation forcing. Regarding materials settings, the default parameters in ENVI-met are not necessarily applicable to anywhere considering that building materials and features are diverse in different regions [25]. This study compared the model predictions using the default and localized parameters in materials, and confirmed the necessity to localize the material parameters for buildings, vegetation and soil. In terms of output intervals, little differences existed among three temporal scales, especially between 10min and 1 h intervals. This result justified that the mobile measurement could be used for ENVI-met model validation, if the measuring instruments fulfill the requirement of accuracy and prevision, and the measurement scheme is scientifically designed.

It is important to note that different variables and locations/sites responded differently towards the model settings. Therefore, if any variable or location needs to be targeted or prioritized, the model settings should be tuned based on research objectives. If there are many targeted locations or variables, some compromises may be made in necessary to ensure a balanced performance.

4.3. Significance and implications of this study

Model evaluation is an essential process for model developers, users, and policy practitioners to gain awareness in the limitations and uncertainties of a specific model. Based on the evaluation results, the model can be improved, invalid conclusions can be avoided, and effective strategies can be developed [68]. To the best of our knowledge, this study is a first attempt to have a systematic evaluation for the recent updates of ENVI-met. Our study also contributes by evaluating the thermal-radiative performance of ENVI-met for three GI typologies simultaneously. Experience of this study is focused on a typical subtropical city; thus, the findings of this study could be transferred to other cities in similar climate background.

For model developers, our study indicated that the latest version of ENVI-met model performed better based on IVS scheme, detailed full forcing scheme, and new ACRT module. Hereafter, potential improvements are expected to provide users flexible selections and detailed instructions in settings. The inputs of cloud forcing need low, medium, and high levels of cloud amounts, when the inputs of radiation forcing need downward direct and diffuse shortwave radiation and downward direct longwave radiation. As weather stations may only provide total cloud amount or global solar radiation [51], introducing a subdivision module for solar radiation and cloud amount would be a convenience for users. Besides, MRT calculation in ENVI-met is different with other models (e.g., RayMan, SOLWEIG) regarding the shape of the standing man [69], therefore it should be helpful for users to select body shape factors based on the research objective. In addition, ENVI-met is deficient in refining mesh for rooftop level, thus leading to larger errors at rooftop than on ground [61]. In order to further investigate the rooftop mitigation strategies, the introduction of vertical mesh refinement in roof level would be very welcomed.

For urban climate researchers, model evaluation and validation are necessary before further applications [67]. According to a comprehensive review of ENVI-met validation studies [6], only 54.74% (52 out of 92 selected studies) have reported the evaluation and validation results. Even among those validated studies, most of them only assessed AT. Other microclimate variables were lacking validation despite of their importance in outdoor thermal comfort and indoor energy saving studies, i.e., only 30.77% assessed MRT prediction, 19.23% validated RH and surface temperature estimation, and 9.62% evaluated wind speed performance [6]. Given these case studies are featured with different background climate, building morphology, surface characteristics, etc., the validation and evaluation results are not transferable among sites. Therefore, it is necessary to validate the model for the targeted research objectives. This study also underscores the necessity of localizing settings regarding the surface features and vegetation characteristics.

For urban planners and policy practitioners, our study can provide valuable information in comprehensive evaluation of ENVI-met performance. Better interpretations in the simulation results are based on a full understanding of both strengths and limitations of the model, so that the planning strategies and policies making can be tailored based on scientific evidence.

4.4. Limitations and further studies

The following limitations of this study should be noted for a better interpretation. First, this study took stationary measurement to collect thermal variables and mobile measurement to obtain radiative variables. Although the differences between 10min and 1 h output intervals were little, future studies could take stationary measurements for radiative variables and compare the results with our study. Second, this study only focused on daytime as the outdoor activities are more intense during diurnal periods. However, considering nighttime UHI phenomenon is even severer, evaluating how ENVI-met model performs in the nocturnal periods is another possible direction. Third, our study was taken in a typical subtropical climate city, whose results may be confined within the cities in similar climate backgrounds. More comprehensive evaluation studies are welcomed in different climate backgrounds. Another important perspective is about the impacts of meteorological conditions on ENVI-met [27]. There is also a need to standardize the distance between weather station for acquiring forcing data and study area. Running nested simulations may be a promising alternative when the distance is too far [70]. Besides, model inter-comparison with other widely used models, i.e., SOLWEIG, RayMan, also needs follow-up studies [26,33].

5. Conclusion

In the coming decades, sustainable urban planning and design will face more intense challenges in the context of climate change and urban overheat. Numerical modelling is a powerful tool to aid urban planners and managers in advancing climate mitigation strategies. ENVI-met, as a microclimate CFD-based model, has been widely used to support climate-sensitive planning. One of the main hypotheses of this kind of application is to interpret the simulation results correctly and comprehensively.

This study was motivated to provide a systematic evaluation of the recent updates of ENVI-met. Besides, how is the performance of ENVI-met to simulate three GI typologies simultaneously is another main focus. Sensitivity analyses were conducted for the inputs and settings of ENVI-met, including new radiation calculation IVS scheme (on and off), meteorological conditions (simple, cloud and radiation forcing), construction surface properties and plant parameters (default and localized settings), and output intervals (10min, 30min, 1 h). Model evaluation was conducted for three GI typologies, nine thermal-radiative parameters, and three output intervals. The simulation results were compared with the data derived from the field measurement based on four evaluation metrics. According to the results, following aspects can be summarized:

- For ENVI-met model settings, models delivered the best performance with full forcing and localized materials. Therefore, localization is necessary for both meteorological boundary conditions and materials. Radiation forcing should be prioritized, while cloud forcing could be alternative if the radiation inputs cannot be acquired. Simple forcing with adjusted solar factors should be avoided in the applications. Moreover, IVS module can improve the model's reliability in estimating radiative variables with around 15% faster speed, although it required higher RAM usage.
- For ENVI-met model performance regarding spatial locations, the model can reproduce different thermal-radiative characteristics among the GI typologies simultaneously, while presenting lower errors on ground sites than at rooftop sites.
- For ENVI-met model performance regarding temporal output intervals, the simulation differences were insignificant, which justified using mobile measurement in model validation on the premise that the measurement campaign is carefully designed.
- For ENVI-met model performance regarding variables, AT and MRT were estimated by ENVI-met with satisfied accuracy, while remaining thermal-radiative variables were reasonably estimated. The prediction of radiative variables was improved by the IVS scheme, and the precision of in-canopy radiation was enhanced by the ACRT module. The accuracy of downward shortwave radiation was highly dependent on the radiative interactions of buildings, plants, and atmosphere, which further affected MRT significantly. Thus, regular-shaped buildings are more recommended for evaluation/validation-oriented measurement.
- For ENVI-met model performance regarding evaluation metrics, the simulation results were sensitive to the metrics. Multiple metrics are suggested in future studies for model validation.

This study emphasized the significance of ENVI-met model valuation before further applications. Radiation forcing and localized settings are necessary to obtain a reliable model. The results of this study indicate the potential directions for model improvement. Besides, this study also helps model users distinguish both the capabilities and limitations of ENVI-met, so that the model result interpretation can be strengthened and urban planning and design strategies can be advanced based on scientific evidence.

CRediT authorship contribution statement

Wanlu Ouyang: Conceptualization, Data curation, Validation, Formal analysis, Methodology, Writing – review & editing, Writing – original draft, Visualization. **Tim Sinsel:** Data curation, Software, Writing – review & editing, Validation. **Helge Simon:** Writing – review & editing, Software. **Tobi Eniolu Morakinyo:** Writing – review & editing. **Huimin Liu:** Writing – review & editing. **Edward Ng:** Funding acquisition, Writing – review & editing.

Declaration of competing interest

The authors declare that they have no known competing financial interests or personal relationships that could have appeared to influence the work reported in this paper.

None.

Acknowledgement

This study is supported by a postgraduate studentship and the "3rd round Vice-Chancellor's Discretionary Fund" from the Chinese University of Hong Kong, and the RGC research grant (No. 14617220) from the Research Grants Council (RGC) of Hong Kong.

Appendix A. Supplementary data S1 and S2

Supplementary data to this article can be found online at https://doi.org/10.1016/j.buildenv.2021.108427.

Appendix

Table A1
Evaluation results of the ENVI-met in previous studies (only evaluation studies were included) *SH: specific humidity; Gflux: ground heat fluxes; AH: absolute humidity; SR: solar radiation. Cfb: Marine West Coast Climate; Cfa: Humid subtropical climate; Af: Tropical rainforest climate; Bwh: Subtropical Desert Climate.*

Ref	Location Period	Model	Climate	Variable	Evaluation metrics						
					R^2	d	RMSE	RMSEs	RMSEu	MAE	MBE
[27]	Bilbao, Spain 6-8th Aug 2010	V4.0	Cfb	AT (°C)	0.92–0.99	0.83–0.94	1–2.07	0.81–2.05	0.28–0.66	0.83–1.82	(−1.54) ~ (−0.17)
[29]	Guangzhou, China 29th Aug. - 2nd Sep 2010	V4.0	Cfa	AT (°C)	0.94	0.97	1.01	0.62	0.79	–	–
				SH (g/kg)	0.52	0.78	0.84	0.55	0.64	–	–
				Gflux (W/m^2)	0.91	0.97	28.3	6	27.6	–	–
[25]	Singapore Oct 2012, Jan, July 2013	V3.1	Af	AT (°C)	0.77–0.98	0.87–0.98	0.52–1.41	0.2–1.37	0.22–0.83	0.40–1.21	(−0.51) ~2.2
				MRT (°C)	0.59–0.8 Day 0–0.83 Night	0.77–0.96 Day 0.11–0.86 Night	6.44–14.1Day 4.29–9.18 Night	1.45–9.56 Day 4.22–9.17 Night	6.24–11.2 Day 0.37–1.06 Night	5.01–12.7 Day 4.22–9.08 Night	(−6.99) ~5.71 Day (−9.08)~ (−4.22) Night
[32]	Berlin, Germany 23 July 2013	V3 V4.0	Cfb	AT (°C)	0.87 V3 0.83–0.98V4	–	1.39 V3 0.96–1.68 V4	–	–	1.13 V3 0.86–1.43 V4	–
				SH (g/kg)	0.1 V3 0.1–0.91 V4	–	1.44 V3 0.35–1.54 V4	–	–	1.31 V3 0.25–1.4 V4	–
				MRT (°C)	0.95 V3 0.94–0.95V4	–	7.98 V3 8.18–8.3 V4	–	–	6.72 V3 6.87–6.9 V4	–
				SW_{down} (W/m^2)	0.91 V3 0.91V4	–	130.46 V3 124.44–128.17 V4	–	–	50.33 V3 47.12–49.7 V4	–
				SW_{up} (W/m^2)	0.6 for both	–	61.86 (V3 84.76–87.12(V4	–	–	39.84 V3 60.04–62.00 V4	–
				LW_{down} (W/m^2)	0.01 V3 0.82–0.86 V4	–	209.6 (V3 115.27–116.32 (V4	–	–	208.03 V3 115.83–114.85 V4	–
				LW_{up} (W/m^2)	0.91 V3 0.92–0.93 V4	–	35.19 (V3 31.7–33.28 (V4	–	–	30.96 V3 27.19–27.62 V4	–
[26]	Arizona, USA Oct. 24, 2014, Feb. 18, 2015, Mar. 23, 2015, June 20, 2015, June 21, 2017	V4.3	Bwh	AT (°C)	0.84–0.9	0.89–0.96	1.45–2.68	0.92–2.36	1.12–1.27	1.39–2.10	(−1.77) ~0.92
				MRT (°C)	0.537–0.765	0.73–0.88	11.17–16.1	1.56–11.95	9.93–14.14	9.66–12.82	(−2.41) ~11.96
[4]	Melbourne, Australia 5–6 Jan 2015	V3.1	Cfb	AT (°C)	–	–	1.01–3.6	–	–	–	–
[33]	Szeged, Hungary 7–8 Aug 2016	V4.4.2	Cfb	MRT (°C)	0.89	0.95	6.92	4.71	5.07	6.26	–
				SW_{down} (W/m^2)	0.94	0.98	78.86	–	–	–	–

(continued on next page)

Table A1 (*continued*)

Ref	Location Period	Model	Climate	Variable	Evaluation metrics R^2	d	RMSE	RMSEs	RMSEu	MAE	MBE
				SW_{up} (W/m^2)	0.33	0.75	40.8	–	–	–	–
				LW_{down} (W/m^2)	0.79	0.9	18.11	–	–	–	–
				LW_{up} (W/m^2)	0.5	0.63	56.65	–	–	–	–
[30]	Sao Paulo, Brazil 2nd 5th April 2016	V4	Cfa	AT (°C)	–	–	0.69–1.9	–	–	–	0.56–1.7
[31]	Guangzhou, China 17, 28-30 Apri. 2017 26–29 July 2017	V4.2	Cfa	AT (°C)	–	0.9–0.92 Spring 0.61–0.7 Summer	1.63–1.68 Spring 2.48–3.97 Summer	1.39 Spring 2.33–3.14 Summer	0.84–0.95 Spring 0.85–2.44 Summer	1.36–1.37 Spring 2.33–3.14 Summer	1.36 Spring 2.33–3.14 Summer
				AH (g/kg)	–	0.95–0.96 Spring 0.68–0.71 Summer	1.34–1.44 Spring 2.4–2.53 Summer	1.15–1.31 Spring 2.09–2.22 Summer	0.6–0.69 Spring 1.19–1.23 Summer	1.11–1.22 Spring 2.11–2.31 Summer	(−1.21) ~ (−1.09) Spring (−2.27) ~2.08 Summer
				SR (W/m2)	–	0.78 Spring 0.87 Summer	255.32 Spring 242.15 Summer	51.7 Spring 15.33 Summer	250.03 Spring 241.65 Summer	44.44 Spring 29.42 Summer	−4.8 Spring 12.26 Summer
This study*	Hong KongSep. 11, 2019	V4.4.6	Cfa	AT (°C)	0.62–0.93	0.68–0.94	0.44–1.63	0.23–1.52	0.28–0.69	0.34–1.38	(−1.34) ~ 0.71
				RH (%)	0.13–0.87	0.28–0.70	3.90–8.58	2.16–8.23	1.41–3.65	3.25–8.15	(−8.15) ~ (−1.15)
				MRT (°C)	0.62–0.87	0.37–0.94	5.74–9.08	3.30–8.18	1.47–6.10	4.34–8.18	1.28–8.18
				SW_{down} (W/m^2)	0.13–0.86	0.32–0.95	41.86–436.68	33.64–313.84	24.92–303.64	33.12–301.56	(−231.70) ~ 136.62
				SW_{up} (W/m^2)	0.08–0.81	0.52–0.94	5.41–49.08	4.26–44.43	3.33–21.09	4.01–39.52	(−39.33) ~ 3.76
				LW_{down} (W/m^2)	0.04–0.77	0.09–0.57	8.55–31.13	7.47–30.97	3.15–8.54	7.00–30.94	(−9.87) ~ 30.94
				LW_{up} (W/m^2)	0.39–0.94	0.11–0.82	15.36–43.54	9.54–43.04	3.60–20.74	12.04–42.64	(−31.67) ~ 42.64
				LW_{in} (W/m^2)	0.67–0.88	0.25–0.47	10.36–33.05	10.25–32.67	1.52–5.02	9.88–31.25	(−9.88) ~ 31.25
				LW_{out} (W/m^2)	0.51–0.67	0.38–0.84	10.98–40.67	3.22–40.65	1.44–10.50	8.51–38.75	(−38.75) ~ (−0.74)

* To be consistent with other studies and ensure the cross-comparison, only the results at 1 h output interval was reported in this table.

Table A2
Validation results of ENVI-met regarding three GI typologies during summer daytime in subtropical climate background (Köppen: Cfa)

GI Typology	Variable	Ref	Evaluation metrics R^2	d	RMSE	RMSEs	RMSEu	MAE	MBE
Green roof	AT (°C)	This study*	0.67	0.88	0.65	0.32	0.57	0.52	−0.29
		[20]	–	–	1.21	–	–	–	–
	RH (%)	This study	0.54	0.63	4.27	3.43	2.55	3.89	−3.40
		[20]	–	–	2.92	–	–	–	–
Bare roof	AT (°C)	This study	0.64	0.70	1.63	1.52	0.59	0.52	−0.29
		[20]	–	–	1.07	–	–	–	–
	RH (%)	This study	0.25	0.70	3.90	2.16	3.25	3.89	−3.40
		[20]	–	–	6.13	–	–	–	–
Green wall	AT (°C)	This study	0.93	0.89	0.56	0.49	0.28	0.52	0.30
		[71]	0.99	–	0.31	–	–	–	–
	RH (%)	This study	0.76	0.60	5.15	4.79	1.88	4.80	−4.71
		[71]	0.98	–	4.09	–	–	–	–
	LWout (W/m^2)	This study	0.67	0.38	40.67	40.65	1.44	38.75	−38.75
		[17]	0.66		42.00				
Bare wall	AT (°C)	This study	0.89	0.94	0.44	0.28	0.34	0.34	−0.20
		[71]	0.99	–	0.35	–	–	–	–
	RH (%)	This study	0.87	0.60	4.95	4.74	1.41	4.68	−4.50
		[71]	0.97	–	4.22	–	–	–	–
	LWout (W/m^2)	This study	0.51	0.84	10.98	3.22	10.50	8.51	−0.74
		[17]	0.7	–	40.70	–	–	–	–
Ground tree	AT (°C)	This study	0.73	0.68	0.96	0.80	0.53	0.85	0.71
		[72]	–	0.91	1.46	–	–	0.77	–

(continued on next page)

Table A2 (*continued*)

GI Typology	Variable	Ref	Evaluation metrics						
			R^2	d	RMSE	RMSEs	RMSEu	MAE	MBE
		[14]	0.81	–	1.00	–	–	–	–
	MRT (°C)	This study	0.67	0.37	5.79	5.60	1.47	5.55	5.55
		[72]	–	0.78	5.21	–	–	4.82	–
		[14]	0.74	–	2.20	–	–	–	–
Tree free	AT (°C)	This study	0.62	0.82	0.73	0.23	0.69	0.61	0.03
		[14]	0.79	–	1.40	–	–	–	–
	MRT (°C)	This study	0.85	0.94	5.74	3.32	4.68	4.34	3.26
		[14]	0.69	–	3.90	–	–	–	–

Note: Referring to the recent review paper [67], only those studies in *Cfa* climate, summer daytime periods, and having detailed measurement illustration were selected. Besides, the measurement conditions in the selected studies were similar with our study, i.e., green roof and bare roof were measured above roof, ground tree was measured under single tree, tree-free site was measured without tree shading.

[*] To be consistent with other studies and ensure the cross-comparison, only the results at 1 h output interval was reported in this table.

References

[1] G. Mills, Urban climatology: history, status and prospects, Urban Clim. 10 (2014) 479–489.
[2] I. Eliasson, The use of climate knowledge in urban planning, Landsc. Urban Plann. 48 (1) (2000) 31–44.
[3] A.J. Arnfield, Two decades of urban climate research: a review of turbulence, exchanges of energy and water, and the urban heat island, Int. J. Climatol. 23 (1) (2003) 1–26.
[4] E. Jamei, et al., Verification of a bioclimatic modeling system in a growing suburb in Melbourne, Sci. Total Environ. 689 (2019) 883–898.
[5] P.A. Mirzaei, F. Haghighat, Approaches to study urban heat island - abilities and limitations, Build. Environ. 45 (10) (2010) 2192–2201.
[6] S. Tsoka, A. Tsikaloudaki, T. Theodosiou, Analyzing the ENVI-met microclimate model's performance and assessing cool materials and urban vegetation applications–A review, Sustain. Cities Soc. 43 (2018) 55–76.
[7] S. Huttner, Further Development and Application of the 3D Microclimate Simulation ENVI-Met, Mainz University, Germany, 2012.
[8] H. Simon, Modeling Urban Microclimate : Development, Implementation and Evaluation of New and Improved Calculation Methods for the Urban Microclimate Model ENVI-Met, 2016.
[9] H. Lee, H. Mayer, L. Chen, Contribution of trees and grasslands to the mitigation of human heat stress in a residential district of Freiburg, Southwest Germany, Landsc. Urban Plann. 148 (2016) 37–50.
[10] W. Ouyang, et al., The cooling efficiency of variable greenery coverage ratios in different urban densities: a study in a subtropical climate, Build. Environ. (2020), 106772.
[11] E. Ng, et al., A study on the cooling effects of greening in a high-density city: an experience from Hong Kong, Build. Environ. 47 (2012) 256–271.
[12] T.E. Morakinyo, et al., Right tree, right place (urban canyon): tree species selection approach for optimum urban heat mitigation - development and evaluation, Sci. Total Environ. 719 (2020), 137461.
[13] T.E. Morakinyo, et al., A study on the impact of shadow-cast and tree species on in-canyon and neighborhood's thermal comfort, Build. Environ. 115 (2017) 1–17.
[14] T.E. Morakinyo, et al., Performance of Hong Kong's common trees species for outdoor temperature regulation, thermal comfort and energy saving, Build. Environ. 137 (2018) 157–170.
[15] Z. Tan, K.K.-L. Lau, E. Ng, Planning strategies for roadside tree planting and outdoor comfort enhancement in subtropical high-density urban areas, Build. Environ. 120 (2017) 93–109.
[16] Z. Tan, K.K.-L. Lau, E. Ng, Urban tree design approaches for mitigating daytime urban heat island effects in a high-density urban environment, Energy Build. 114 (2016) 265–274.
[17] T.E. Morakinyo, et al., Thermal Benefits of Vertical Greening in a High-Density City: Case Study of Hong Kong, Urban Forestry & Urban Greening, 2019.
[18] J.A. Acero, et al., Thermal impact of the orientation and height of vertical greenery on pedestrians in a tropical area, in: Building Simulation, Springer, 2019.
[19] T.E. Morakinyo, et al., Temperature and cooling demand reduction by green-roof types in different climates and urban densities: a co-simulation parametric study, Energy Build. 145 (2017) 226–237.
[20] C. Jin, et al., Effects of green roofs' variations on the regional thermal environment using measurements and simulations in Chongqing, China, Urban For. Urban Green. 29 (2018) 223–237.
[21] G. Zhang, et al., Impact of morphological characteristics of green roofs on pedestrian cooling in subtropical climates, Int. J. Environ. Res. Publ. Health 16 (2) (2019) 179.
[22] U. Berardi, The outdoor microclimate benefits and energy saving resulting from green roofs retrofits, Energy Build. 121 (2016) 217–229.
[23] L.S. Matott, J.E. Babendreier, S.T. Purucker, Evaluating uncertainty in integrated environmental models: a review of concepts and tools, Water Resour. Res. 45 (6) (2009).
[24] D.G. Fox, Judging air quality model performance: a summary of the AMS workshop on dispersion model performance, woods hole, Mass., 8–11 September 1980, Bull. Am. Meteorol. Soc. 62 (5) (1981) 599–609.
[25] M. Roth, V.H. Lim, Evaluation of canopy-layer air and mean radiant temperature simulations by a microclimate model over a tropical residential neighbourhood, Build. Environ. 112 (2017) 177–189.
[26] P.J. Crank, et al., Validation of seasonal mean radiant temperature simulations in hot arid urban climates, Sci. Total Environ. 749 (2020), 141392.
[27] J.A. Acero, J. Arrizabalaga, Evaluating the performance of ENVI-met model in diurnal cycles for different meteorological conditions, Theor. Appl. Climatol. 131 (1) (2018) 455–469.
[28] J.A. Acero, K. Herranz-Pascual, A comparison of thermal comfort conditions in four urban spaces by means of measurements and modelling techniques, Build. Environ. 93 (2015) 245–257.
[29] X. Yang, et al., Evaluation of a microclimate model for predicting the thermal behavior of different ground surfaces, Build. Environ. 60 (2013) 93–104.
[30] P. Shinzato, et al., Calibration process and parametrization of tropical plants using ENVI-met V4–Sao Paulo case study, Architect. Sci. Rev. 62 (2) (2019) 112–125.
[31] Z. Liu, S. Zheng, L. Zhao, Evaluation of the ENVI-met vegetation model of four common tree species in a subtropical hot-humid area, Atmosphere 9 (5) (2018) 198.
[32] B. Jänicke, et al., Evaluating the effects of façade greening on human bioclimate in a complex urban environment, Adv. Meteorol. 2015 (2015).
[33] C.V. Gál, N. Kántor, Modeling mean radiant temperature in outdoor spaces, A comparative numerical simulation and validation study, Urban Clim. 32 (2020), 100571.
[34] ENVI-met, New features winter-release 2018/2019 https://www.envi-met.com/wp-content/uploads/2019/07/ENVI-met-new-features-winter-release-2018.pdf [Accessed on *18 03 2020*].
[35] L.L.H. Peng, et al., Cooling effects of block-scale facade greening and their relationship with urban form, Build. Environ. 169 (2020), 106552.
[36] B. Abdi, A. Hami, D. Zarehaghi, Impact of small-scale tree planting patterns on outdoor cooling and thermal comfort, Sustain. Cities Soc. 56 (2020), 102085.
[37] D. Shi, et al., Synergistic cooling effects (SCEs) of urban green-blue spaces on local thermal environment: a case study in Chongqing, China, Sustain. Cities Soc. 55 (2020), 102065.
[38] H. Simon, et al., Modeling transpiration and leaf temperature of urban trees–a case study evaluating the microclimate model ENVI-met against measurement data, Landsc. Urban Plann. 174 (2018) 33–40.
[39] ENVI-met, Features: green & blue technologies https://www.envi-met.com/features/[Accessed on *18 03 2020*].
[40] W. Ouyang, et al., Thermal-irradiant performance of green infrastructure typologies: field measurement study in a subtropical climate city, Sci. Total Environ. 764 (2021), 144635.
[41] A. Middel, E.S. Krayenhoff, Micrometeorological determinants of pedestrian thermal exposure during record-breaking heat in Tempe, Arizona: introducing the MaRTy observational platform, Sci. Total Environ. 687 (2019) 137–151.
[42] C.D. Ziter, et al., Scale-dependent interactions between tree canopy cover and impervious surfaces reduce daytime urban heat during summer, Proc. Natl. Acad. Sci. Unit. States Am. 116 (15) (2019) 7575–7580.
[43] HKO, Monthly Meteorological Normals for Hong Kong. https://www.hko.gov.hk/en/cis/normal/1981_2010/normals.htm [Accessed on April 2021].
[44] Hong Kong SAR, Greening Master Plan, Hong Kong Civil Engineering and Development Department, 2004.
[45] Hong Kong SAR, Practice Note for Authorized Persons, Registered Structural Engineers and Registered Geotechnical Engineers (APP-152), Hong Kong Buidling Department, 2016.
[46] F. Salata, et al., Urban microclimate and outdoor thermal comfort. A proper procedure to fit ENVI-met simulation outputs to experimental data, Sustain. Cities Soc. 26 (2016) 318–343.
[47] E. Burton, Measuring urban compactness in UK towns and cities, Environ. Plann. Plann. Des. 29 (2) (2002) 219–250.
[48] S. Kotthaus, et al., Derivation of an urban materials spectral library through emittance and reflectance spectroscopy, ISPRS J. Photogrammetry Remote Sens. 94 (2014) 194–212.

[49] J. Yang, et al., A semi-empirical method for estimating complete surface temperature from radiometric surface temperature, a study in Hong Kong city, Rem. Sens. Environ. 237 (2020), 111540.

[50] HKO, Summary of meteorological and tidal observations in Hong Kong, 2019. https://www.hko.gov.hk/tc/publica/smo/files/SMO2019.pdf.

[51] P. Weihs, et al., The uncertainty of UTCI due to uncertainties in the determination of radiation fluxes derived from measured and observed meteorological data, Int. J. Biometeorol. 56 (3) (2012) 537–555.

[52] A. Saltelli, et al.. *Sensitivity analysis in practice: a guide to assessing scientific models* vol. 1, Wiley Online Library, 2004.

[53] D.N. Moriasi, et al., Model evaluation guidelines for systematic quantification of accuracy in watershed simulations, Trans. ASABE 50 (3) (2007) 885–900.

[54] C.J. Willmott, Some comments on the evaluation of model performance, Bull. Am. Meteorol. Soc. 63 (11) (1982) 1309–1313.

[55] C.J. Willmott, On the validation of models, Phys. Geogr. 2 (2) (1981) 184–194.

[56] M. Stunder, S. Sethuraman, A statistical evaluation and comparison of coastal point source dispersion models, Atmos. Environ. 20 (2) (1967) 301–315, 1986.

[57] E. Krüger, F. Minella, A. Matzarakis, Comparison of different methods of estimating the mean radiant temperature in outdoor thermal comfort studies, Int. J. Biometeorol. 58 (8) (2014) 1727–1737.

[58] Y.-C. Chen, T.-P. Lin, A. Matzarakis, Comparison of mean radiant temperature from field experiment and modelling: a case study in Freiburg, Germany, Theor. Appl. Climatol. 118 (3) (2014) 535–551.

[59] Y. Wang, J. Zacharias, Landscape modification for ambient environmental improvement in central business districts–a case from Beijing, Urban For. Urban Green. 14 (1) (2015) 8–18.

[60] H. Simon, T. Sinsel, M. Bruse, Advances in simulating radiative transfer in complex environments, Appl. Sci. 11 (12) (2021) 5449.

[61] P.J. Crank, et al., Evaluating the ENVI-met microscale model for suitability in analysis of targeted urban heat mitigation strategies, Urban Clim. 26 (2018) 188–197.

[62] H. Simon, T. Sinsel, M. Bruse, Introduction of fractal-based tree digitalization and accurate in-canopy radiation transfer modelling to the microclimate model ENVI-met, Forests 11 (8) (2020) 869.

[63] T.E. Morakinyo, et al., Modelling the effect of tree-shading on summer indoor and outdoor thermal condition of two similar buildings in a Nigerian university, Energy Build. 130 (2016) 721–732.

[64] N. Müller, W. Kuttler, A.-B. Barlag, Counteracting urban climate change: adaptation measures and their effect on thermal comfort, Theor. Appl. Climatol. 115 (1) (2014) 243–257.

[65] Y. Wang, U. Berardi, H. Akbari, Comparing the effects of urban heat island mitigation strategies for Toronto, Canada, Energy Build. 114 (2016) 2–19.

[66] G. Kyriakodis, M. Santamouris, Using reflective pavements to mitigate urban heat island in warm climates-Results from a large scale urban mitigation project, Urban Clim. 24 (2018) 326–339.

[67] Z. Liu, et al., Heat mitigation benefits of urban green and blue infrastructures: a systematic review of modeling techniques, validation and scenario simulation in ENVI-met V4, Build. Environ. (2021), 107939.

[68] A.J. Jakeman, R.A. Letcher, J.P. Norton, Ten iterative steps in development and evaluation of environmental models, Environ. Model. Software 21 (5) (2006) 602–614.

[69] B. Holmer, F. Lindberg, S. Thorsson, Mean radiant temperature and the shape of the standing man. 10th International Conference on Urban Climate/14th Symposium on the Urban Environment, New York, US, 2018.

[70] H. Simon, et al., Downscaling climate models: running nested simulations in the microclimate model ENVI-met. Passive and Low Energy Architecture, Hong Kong, 2018.

[71] L.L. Peng, et al., Energy savings of block-scale facade greening for different urban forms, Appl. Energy 279 (2020), 115844.

[72] L. Zhang, Q. Zhan, Y. Lan, Effects of the tree distribution and species on outdoor environment conditions in a hot summer and cold winter zone: a case study in Wuhan residential quarters, Build. Environ. 130 (2018) 27–39.